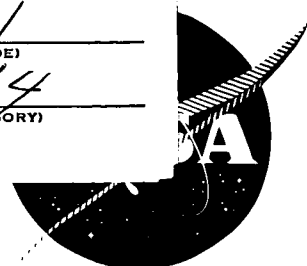


(ACCESSION NUMBER)  
115  
(PAGES)

(THRU)  
1  
(CODE)

NASA CR OR TMX OR AS NUMBER  
N66-14225

14  
(CATEGORY)



NASA CR-54763

(SIXTH QUARTERLY REPORT)  
PRESSURE MEASURING SYSTEMS FOR  
CLOSED CYCLE LIQUID METAL FACILITIES

PO PRICE \$

CFSTI PRICE(S) \$

Anthony J. Cassano

Hard copy (HC) 4.00

Microfiche (MF) .75

1963 July 65

PREPARED FOR  
NATIONAL AERONAUTICS AND SPACE ADMINISTRATION  
CONTRACT NAS 3-4170

October 18, 1965

Consolidated Controls Corporation  
Bethel, Connecticut

A SUBSIDIARY OF  CORPORATION

## NOTICE

This report was prepared as an account of Government sponsored work. Neither the United States, nor the National Aeronautics and Space Administration (NASA), nor any person acting on behalf of NASA:

- A.) Makes any warranty or representation, expressed or implied, with respect to the accuracy, completeness, or usefulness of the information contained in this report, or that the use of any information, apparatus, method, or process disclosed in this report may not infringe privately owned rights; or
- B.) Assumes any liabilities with respect to the use of, or for damages resulting from the use of any information, apparatus, method or process disclosed in this report.

As used above, "person acting on behalf of NASA" includes any employee or contractor of NASA, or employee of such contractor, to the extent that such employee or contractor of NASA, or employer of such contractor prepares, disseminates, or provides access to, any information pursuant to his employment or contract with NASA, or his employment with such contractor.

Requests for copies of this report should be referred to:

National Aeronautics and Space Administration  
Scientific and Technical Information Facility  
P. O. Box 33  
College Park, Md., 20740



SIXTH QUARTERLY REPORT  
June 1, 1965-August 31, 1965

PRESSURE MEASURING SYSTEMS FOR  
CLOSED CYCLE LIQUID METAL FACILITIES

PREPARED FOR  
NATIONAL AERONAUTICS AND SPACE ADMINISTRATION

CONTRACT NAS 3-4170

October 18, 1965

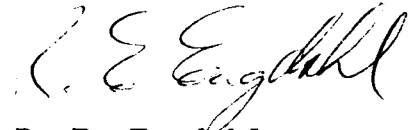
Technical Management  
NASA - Lewis Research Center  
Nuclear Power Technology Branch  
R. N. Weltmann

Prepared by:



Anthony J. Cassano  
Research Physicist

Approved:



R. E. Engdahl  
Project Manager

Consolidated Controls Corporation  
Bethel, Connecticut

## FOREWORD

The major contributors to this development program are Mr. R. Engdahl, Project Manager, Mr. Anthony Cassano, Mr. David Mends, Mr. Philip Tubman and Mr. George Garrity. Analysis and presentation of the metallographic and X-ray microprobe data contained in this report was performed by Mr. David Mends and Mr. Philip Tubman.

ABSTRACT

14205  
Continuing development of a thermionic diode pressure transducer for liquid metal applications is described. Two test models were fabricated and installed in the Vacuum Test Facility. One of the models incorporated the C-129Y double convolution pressure capsule previously tested using the optical technique. A cross-sectional cut was made of the representative Nb-1Zr/Lucalox seal which recently underwent life testing. Analysis of the cross-section indicates that seals fabricated by this technique will meet the performance requirements for temperature and internal pressurization. The 500 hour potassium compatibility test was completed. After the test, the four test pressure capsules were found to be still leak tight. Metallographic examination showed no evidence of potassium attack in the capsule interior. Initial work on the transducer signal conditioning equipment established the various functional blocks of the system. The differential pressure transducer effort was concentrated on experimental work involving the force-deflection and frequency response characteristics of a representative mechanical linkage.

*Author*

## TABLE OF CONTENTS

<u>Section</u>	<u>Title</u>	<u>Page No.</u>
	Abstract	i
	Table of Contents	ii
	List of Illustrations	iii
	List of Tables	vi
1.0	Introduction	1
2.0	Summary	2
3.0	Thermionic Diode Pressure Transducer	4
3.1	Transducer Frequency Response Characteristics	8
4.0	Metal-Ceramic Seal Evaluation	15
4.1	Metallographic Analysis	17
4.2	X-Ray Microprobe Analysis	24
5.0	Compatibility Test Program	30
5.1	Examination of the Test Capsules	31
5.2	Potassium Analysis	37
6.0	Transducer Signal Conditioning	43
7.0	Differential Pressure Transducer	46
	References	93
	Appendix A - Transducer Frequency Response	94
	Appendix B - Nomenclature	105

## LIST OF ILLUSTRATIONS

<u>NO.</u>	<u>TITLE</u>	<u>PAGE NO.</u>
1a.	Basic Pressure Transducer System	51
1b.	Pressure Transducer System with Snubber	51
2	Transducer Natural Frequency Characteristics	52
3	Transducer Damping Characteristics	53
4	Transducer Phase Shift Characteristics	54
5	Transducer Amplitude Ratio Characteristics	55
6	Representative Nb-1Zr/Lucalox Seal	56
7	Ceramic to Metal Seal, Tube End, 100X	57
8	Ceramic to Metal Seal, Tube End, 100X	58
9	Tube End Interface, 500X	59
10	Tube End Metal Member, 200X	60
11	Ceramic to Metal Seal Tube End, 100X	61
12	Tube End Metal Member, 200X	62
13	Tube End Interface, 500X	63
14	Bulged End Central Portion, 200X	64
15	Ceramic to Metal Seal Bulged End, 100X	65
16	Bulged End Metal Member, 200X	66
17	Bulged End Metal Member, 200X	67
18	Bulged End Interface, 500X	68

# LIST OF ILLUSTRATIONS (Cont'd)

<u>NO.</u>	<u>TITLE</u>	<u>PAGE NO.</u>
19	Bulged End Interface, 500X	69
20	Nb-Ti X-ray Microprobe Traces	70
21	Ni-Al X-ray Microprobe Traces	71
22	W-Y X-ray Microprobe Traces	72
23	Terminal Compatibility Capsule	73
24	C-129Y Compatibility Capsule	74
25	FS-85 Compatibility Capsule	75
26	T-222 Compatibility Capsule	76
27	W-25Re Compatibility Capsule	77
28	Lower Portion of Terminal Compatibility Capsule	78
29	Electrical Terminals	79
30	C-129Y Compatibility Capsule Photograph	80
31	FS-85 Compatibility Capsule Photograph	81
32	T-222 Compatibility Capsule Photograph	82
33	W-25Re Compatibility Capsule Photograph	83
34	C-129Y Compatibility Capsule Micro-Photograph	84
35	FS-85 Compatibility Capsule Micro-Photograph	85
36	T-222 Compatibility Capsule Micro-Photograph	86
37	W-25Re Compatibility Capsule Micro-Photograph	87

# LIST OF ILLUSTRATIONS (Cont'd)

<u>NO.</u>	<u>TITLE</u>	<u>PAGE NO.</u>
38	Intergrannular Crack in T-222 Compatibility Capsule	88
39	Transducer Signal Conditioning Block Diagram	89
40	Differential Pressure Transducer Configuration	90
41	Differential Pressure Transducer Deflection Characteristics	91
42	Differential Mock-up Force-Deflection Characteristics	92

## LIST OF TABLES

<u>No.</u>	<u>Title</u>	<u>Page No.</u>
1	Density and Viscosity Values for Some Selected Fluids	11
2	Metallographic Photo-Indexing System	18
3	Potassium Analysis Before and After Compatibility Test	38



## 1.0

### Introduction

The objective of this program is to develop pressure transducers which can be used in advanced closed cycle power systems using liquid metals such as mercury, sodium, potassium and other alkali metals as working and heat transfer media at elevated temperatures.

Accurate pressure measurements in the high temperature liquid, vapor, and two phase streams are required for research, design and control purposes. In addition, space flight requires lightweight systems capable of enduring long periods of unattended operation.

Liquid metal pressure measurements at elevated temperatures pose many design problems demanding the best from available materials. To establish a firm design base for the transducer equipment, four diaphragm materials and two transducer systems have been chosen for evaluation. The selected transducer system using a thermionic diode sensor will be developed for use as either ground or flight hardware for measuring absolute and differential pressures. The absolute pressure instrument will be developed for a full scale range of 80 psia and the differential instrument for  $\pm 5$  psid.

## 2.0

### Summary

During the report period, two thermionic diode sensors were fabricated and installed in the Vacuum Test Facility. One test device incorporated the micrometer head fixture to control the motion of a simulated active collector. The second test device incorporated the C-129Y double convolution pressure capsule. Only limited results have been obtained because of faulty braze joints between the emitter housing and the Lucalox ceramic base. The two test units were rebuilt using wires, brazed into the Lucalox base, to secure the emitter housing.

A cross-section of the representative Nb-1Zr/Lucalox seal, which recently underwent a 2400 hour life test at 1800°F and various internal pressure levels, was successfully prepared. Both photographic and micro-probe techniques were used to analyze the cross-section. Results indicate that seals fabricated by this technique will meet the temperature (1800°F) and internal pressurization (160 psia) requirements.

The 500 hour potassium compatibility test was completed. The potassium was extracted from the test capsules and metallographic examination of the capsules was performed. The four single convolution pressure capsules (C-129Y, FS-85, T-222 and W-25Re) were found to be leak tight after the compatibility testing and there was no evidence of potassium attack in the capsule interior. One of the four electrical terminals developed a leak during the testing.

The various functional blocks of the transducer signal conditioning system have been established. The signal levels are quite reasonable and the necessary system components are readily available. Initial bread-board fabrication of the system components is underway.

A welded mock-up of a differential pressure transducer mechanical configuration was fabricated. Tests were performed to evaluate the force-deflection and frequency response characteristics of the configuration.

### 3.0 Thermionic Diode Pressure Transducer

To avoid confusion in discussing the transducer test units now being evaluated and those planned for future testing, the transducers will be referred to in numerical order (i.e., T-1, T-2, etc). T-1 was described in the Fifth Quarterly Report (Reference 1). This unit used a tungsten heater with molybdenum external leads. The heater wire was wound on an alumina coil form and the tungsten/molybdenum connection was made by plasma-spraying the joint with tungsten. During preliminary testing in the Vacuum Test Facility, the heater of T-1 developed an open circuit, apparently in the first heater turn around the coil form, which includes one of the plasma-sprayed joints. Efforts to disassemble the heater to determine the exact cause of failure were unsuccessful.

The use of rhenium wire for both the heater and the external leads was discussed in the Fifth Quarterly Report (Reference 1). To implement this plan, both 0.010 inch and 0.012 inch diameter rhenium wire was

obtained for the external leads and a heater design was developed using 0.003 inch diameter rhenium wire. Wire embrittlement and breakage problems encountered in the fabrication of the heater indicated that the development of the pure rhenium heater would take too long to be of value in the program. As a second choice, heaters of 0.003 inch diameter W-3Re wire were ordered. Until these heaters were received, work continued using the tungsten heater and the rhenium external leads.

During the report period, two transducer test units, T-2 and T-3, were fabricated and installed in the Vacuum Test Facility. Both devices contained a pure tungsten heater with rhenium external leads. T-2 used 0.010 inch diameter rhenium wire; T-3 used 0.012 inch diameter rhenium wire. The tungsten/rhenium connection was welded and appeared much stronger than the plasma-sprayed tungsten/molybdenum connection used in T-1.

The T-2 unit incorporated the micrometer head fixture to control the motion of a simulated active collector.

Initial bake-out in the Vacuum Test Facility was completed and emitter activation indicated that the emission currents from both emitters were close to the values predicted by space charge theory. After bake-out, the active and reference collector currents became erratic, forcing suspension of the test and removal of the unit to determine the cause of the problem.

The T-3 unit consisted of the thermionic diode sensor installed inside the C-129Y double convolution pressure capsule. The C-129Y capsule was modified to allow for argon pressurization of the T-3 unit in the Vacuum Test Facility. The C-129Y capsule had undergone the original deflection test program using the optical technique. The results obtained from the optical measurements will be compared to those obtained by using the thermionic diode sensor. Following the initial bake-out, an electrical short was observed between the C-129Y capsule and the emitter housing of the thermionic sensor. The unit was removed from the vacuum chamber and dismantled.

In both the T-2 and T-3 units, faulty braze joints were found between the emitter housing and the Lucalox ceramic base. The resultant cocking of the emitter housing on the Lucalox base caused the erratic data of T-2 and the short circuit in T-3. In addition, hairline cracks were noticed at the base of the Lucalox posts upon which the emitter housing was mounted. To resolve these problems, it was decided to move the position of the Lucalox posts so that each post had a central hole. Previously, the holes had been used to contain the wiring to the thermionic diode sensor. Reinforcing wires were placed in the holes and brazed in place. Enough of the wire extended out the top of the posts to mechanically hold down the mounting tabs of the emitter housing. For added structural integrity, the wire was brazed to the mounting tab.

Two new Lucalox bases, incorporating the reinforcing wires, were prepared for use in T-2 and T-3. During re-assembly of the T-3 unit, the heater developed an open-circuit inside the casting, requiring the

preparation of a new encapsulated heater assembly. At this time, the W-3Re heaters had been obtained and were used with 0.012 inch diameter rhenium external leads. The new heater exhibited good ductility during assembly and the W-3Re/rhenium weld joint appeared sound. The T-2 unit was re-assembled with its original pure tungsten heater assembly described previously.

Both T-2 and T-3 were installed in the Vacuum Test Facility and are undergoing initial bake-out.

### 3.1 Transducer Frequency Response Characteristics

The basic problem for a measuring system consisting of a pressure source and a pressure transducer connected by a simple tube (Figure 1a) is that the piping system is highly underdamped when the system is designed for high frequency response. One of the corrective steps is to increase the damping by reducing the pipe diameter. This method, however, severely lowers the natural frequency of the transducer assembly. In practice it is common to solve this problem by installing some type of "snubber" between the pressure source



and the transducer to increase the damping and still provide the total flow area required to maintain the desired natural frequency.

A possible model of such a snubber is a group of parallel tubes which connect the pressure source to the pressure transducer. The schematic of this model is shown in Figure 1b, and the equations A24 and A26, derived in Appendix A, present the natural frequency and damping ratio terms.

From equations A24 and A26 it will be noted that the various terms which are used to calculate the natural frequency and the damping coefficient have been grouped according to their availability. For the natural frequency calculation the first term is  $\sqrt{\frac{3\Delta P/\Delta V}{64\pi}}$  which includes the values associated with the transducer. Once this term is calculated for a particular transducer, it need not be changed for any application problem. The second group is representative of the fluid  $\left(\frac{1}{\rho}\right)$  to be measured and is also fixed for a given application. The last

term  $d\sqrt{\frac{N}{L}}$  contains the variables connecting the pressure source to the transducer. This term must be adjusted to meet the frequency response requirements.

Similarly, the damping coefficient, equation A26, contains three similar terms:

$$\left( 16\sqrt{\frac{3}{\pi\left(\frac{\Delta P}{\Delta V}\right)}} \right), \left( \frac{\mu}{\sqrt{\rho}} \right), \text{ and } \left( \frac{1}{d^3} \sqrt{\frac{L}{N}} \right)$$

Figures 2 and 3 are graphical representations of the natural frequency and damping coefficients based on the above selected terms for the 80 psia transducer being constructed. As an aid to selecting the parameter range, Table 1 was prepared to provide typical values. Table 1 should also be helpful in demonstrating the dimensional units used in these equations.

As a sample of how this data can be used, an example will now be presented. Let us assume that the piping system is to have a natural frequency of 500 cps, a

TABLE 1

## DENSITY AND VISCOSITY VALUES FOR SOME SELECTED FLUIDS

The units used in this work are those in Columns 3 and 5.

1.	2.	3.	4.	5.	6.	7.
Fluid and Temp.	$\mu$ Viscosity Slugs/ft-sec or #f-sec/ft <sup>2</sup>	$\mu$ Viscosity #f-sec in <sup>2</sup>	$\rho$ Density Slugs/ft <sup>3</sup> or #f-sec <sup>2</sup> /ft <sup>4</sup>	$\rho$ Density #f-sec <sup>2</sup> in <sup>4</sup>	$\sqrt{\rho}$	$\frac{\mu}{\sqrt{\rho}}$
Water 0°C 100°C	3.75 x 10 <sup>-5</sup> .59 x 10 <sup>-5</sup>	2.6 x 10 <sup>-7</sup> 0.41 x 10 <sup>-7</sup>	1.94 1.86	.94 x 10 <sup>-4</sup> .9 x 10 <sup>-4</sup>	.97 x 10 <sup>-2</sup> .95 x 10 <sup>-2</sup>	2.68 x 10 <sup>-5</sup> .43 x 10 <sup>-5</sup>
Mercury 0°C	3.51 x 10 <sup>-5</sup>	2.44 x 10 <sup>-7</sup>	26.29	12.7 x 10 <sup>-4</sup>	3.57 x 10 <sup>-2</sup>	.68 x 10 <sup>-5</sup>
Air 59°C	3.7 x 10 <sup>-7</sup>	2.57 x 10 <sup>-9</sup>	.0024	1.16 x 10 <sup>-7</sup>	3.4 x 10 <sup>-4</sup>	.76 x 10 <sup>-5</sup>
Heavy Lube Oil R.T. Nominal	1.0 x 10 <sup>-2</sup>	.7 x 10 <sup>-4</sup>	1.68	.81 x 10 <sup>-2</sup>	.9 x 10 <sup>-2</sup>	.78 x 10 <sup>-2</sup>
Potassium 1292°F	.91 x 10 <sup>-4</sup>	.63 x 10 <sup>-6</sup>	1.31	.63 x 10 <sup>-4</sup>	.8 x 10 <sup>-2</sup>	2.47 x 10 <sup>-6</sup>

damping coefficient of 0.05 and a tube length of 1 inch from pressure source to pressure transducer; and that the fluid is liquid potassium with a density of  $0.63 \times 10^{-4}$  lb-sec<sup>2</sup>/in<sup>4</sup> and a viscosity of  $0.63 \times 10^{-6}$  lb-sec/in<sup>2</sup>.

From Figure 2, using  $\rho = 0.63 \times 10^{-4}$  and  $f_n = 500$  cps, the value of  $d\sqrt{\frac{N}{L}} = 0.17$ . Similarly, from Figure 3 for  $\frac{\mu}{\sqrt{\rho}} = \frac{0.63 \times 10^{-6}}{\sqrt{0.63 \times 10^{-4}}} = 7.94 \times 10^{-5}$  and  $h = 0.05$ , the value of  $\frac{1}{d^3} \sqrt{\frac{L}{N}} = 7.5 \times 10^3$ .

Since the tube length is 1 inch, these relations reduce to:

$$d\sqrt{N} = 0.17 \text{ or } d = \frac{0.17}{\sqrt{N}}$$

$$\text{and } \frac{1}{d^3 \sqrt{N}} = 7.5 \times 10^3$$

By substitution, values for  $d$  and  $N$  may be obtained

$$d^3 = \frac{4.9 \times 10^{-3}}{N^{3/2}}$$

$$\text{and } N = (7.5 \times 10^3) (4.9 \times 10^{-3}) \approx 37$$

$$d = \frac{0.17}{\sqrt{37}} = 0.028 \text{ inch}$$

This problem demonstrates how the multitube pressure transmission model allows a solution which satisfies both the natural frequency and damping ratio requirements. With this solution, the phase angle and attenuation values can be determined from standard curves such as presented in Figures 4 and 5.

As a check on the assumption that the mass of the transducer is negligible and therefore can be neglected, the transducer natural frequency can be computed by the following:

$$f_n = \frac{1}{2\pi} \sqrt{\frac{\left(\frac{\Delta P}{\Delta V}\right) A^2}{M_1}}$$

For our case,

$$\Delta P = 80 \text{ psi}$$

$$\Delta V = \frac{\pi (1.7)^2 10^{-3}}{4} = 2.27 \times 10^{-3} \text{ in}^3$$

$$A = \frac{\pi (1.7)^2}{4} = 2.27 \text{ in}^2$$

$$M_1 = 0.84 \times 10^{-3} \text{ lb-sec}^2/\text{in} \text{ (assuming W-25Re material)}$$

$$\text{and } f_n = 2340 \text{ cps}$$

This frequency for the transducer is enough above 500 cps so that the above assumptions are justified. However, the transducer would become the limiting factor if piping frequencies close to the transducer natural frequency were to be considered.

#### 4.0 Metal-Ceramic Seal Evaluation

The metal-ceramic joining technique proposed for use in the transducer was tested to failure as described in the Fifth Quarterly Report (Reference 1). The test sample contained seals between Lucalox and Nb-1Zr. The Lucalox was metallized with a tungsten/yttria compound and brazed with a nickel/niobium/titanium alloy. A sketch of the test seal section after test is shown in Figure 6.

The seal was put on test in the Vacuum Test Facility with an adaption to permit the application of internal pressure. The pressure was developed using high purity argon.

The life testing was conducted in a series of step increases of internal pressure after the assembly had been brought to 1800°F and leak-checked at the 10<sup>-9</sup> torr level by monitoring the Vacuum Test Facility pressure. Prior to these tests, the seal was pressure cycled between 0-500 psia at room temperature, 500, 1000, 1200, 1400, 1600 and 1800°F.

The extended life testing sequence was as follows:

1000	hours	at	500	psia
100	"	"	600	psia
100	"	"	700	psia
100	"	"	800	psia
100	"	"	900	psia
1000	"	"	1000	psia

At the end of the extended life test the seal was still intact and preparations were being made to raise the temperature above 1800°F when the pressurizing tube failed.

As seen in Figure 6 the failure occurred in the distended pressurizing tube which had been re-crystallized by the heliarc welding. The seal was removed from the test fixture and microscopically examined. The location of the leak was determined by helium leak check and then pin-pointed by internal pressure and soap bubble technique.

The two bulged end plates and distended tube were measured to determine the amount of movement which



had taken place. The center of the lower end plate had been displaced 0.010 inch. The upper end plate with welded tube had been displaced 0.022 inch. The pressure tube had distended in the recrystallized area from 0.090 inch OD to 0.107 inch OD. Its wall thickness was thinned in the area of failure from 0.007 to 0.003 inch.

#### 4.1 Metallographic Analysis

The seal was sectioned and prepared for metallographic examination. Photomicrographs were taken of various areas of the section.

The areas of the seal that are shown in the photomicrographs are indicated in Figure 6. The photomicrographs are shown in Figures 7 to 19 inclusive. They have been arranged in 4 groups as indicated in Table 2.

The photomicrographs of the metal-ceramic interface of the upper end plate are shown in Figures 7 to 13 and represent areas I and II of Figure 6. The Nb-1Zr end plate is shown with a portion of the bonded Lucalox on each side. The Lucalox appears black in the photos.

TABLE 2  
Metallographic Photo-Indexing System  
(Areas Refer to Section Shown in Figure 6)

Figure No.	Position in Seal	Seal Area	Magnification	Remarks
7	Tube plate, right hand	I	100 X	Whole Cross Section
8	Tube plate, right hand	I	100 X	Whole Cross Section
9	Tube plate, right hand	I	500 X	Metal/Ceramic Interface
10	Tube plate, right hand	I	200 X	Whole Cross Section
11	Tube plate, left hand	II	100 X	Whole Cross Section
12	Tube plate, left hand	II	200 X	Whole Cross Section
13	Tube plate, left hand	II	500 X	Metal/Ceramic Interface
14	Blank end, center	III	200 X	Metal Only
15	Blank end, right hand	IV	100 X	Whole Cross Section
16	Blank end, right hand	IV	200 X	Whole Cross Section, Inside Edge of Ceramic
17	Blank end, right hand	IV	200 X	Whole Cross Section, Inside Edge of Ceramic
18	Blank end, right hand	IV	500 X	Metal/Ceramic Interface
19	Blank end, right hand	IV	500 X	Metal/Ceramic Interface, Enlargement "Dodged" to Show Ceramic Detail

In traversing from Lucalox to the Nb-1Zr member the following seal components are present:

1. Lucalox
2. Tungsten metallizing
3. Glass and crystal inclusions
4. Reaction zone between tungsten metallizing and Nb-1Zr
5. Nb-1Zr

Area III is represented in Figure 14 which shows the central portion of the lower end plate bulged 0.010 inch during test.

Figures 15 and 19 show photomicrographs of Area IV as indicated in Figure 6.

As in Area I, area IV shows the Nb-1Zr brazed between the two Lucalox members. Figures 16 and 17 in particular show the metal-ceramic joint at the inside surfaces of the two lower Lucalox rings. They are adjacent fields, and if placed together at reference marks, form a continuous photo.

Figures 17 and 19 show portions of Figure 15 at 200 X and 500 X magnification, respectively. Figure 19 was printed by "dodging" or shading the negative during printing so as to reveal the structure of the Lucalox as well as that of the metal. This particular section was selected for the X-ray microprobe traverse described in a later section of this report.

By comparing the relative grain sizes of the Nb-1Zr tube plate (Figures 10 and 12) and blank end plate (Figure 14) it is seen that there is a marked disparity between the two pieces. The grain size in the blank end plate (Figure 14) is non-uniform but falls in the range 0.001 to 0.008 inch diameter. On the other hand, in the tube plate (Figures 10 and 12) the grains are so enlarged that the 0.018 inch thick Nb-1Zr sheet is essentially one grain thick. However, there are a few much smaller grains on one surface of the metal. The enlarged grain growth is considered to have occurred during the heliarc welding of the tube to the tube plate. The layer of small grains is due to the presence of surface contamination,

probably oxygen, which exerted an inhibiting effect on grain growth. The smaller overall grain size in the blank end plate presumably occurred during annealing when brazing the assembly.

The structure of the actual metal-ceramic joints is rather complex. The layers adjacent to the Lucalox (the Lucalox appears black in all the Figures except Figure 19) originally consisted of a tungsten/yttria powder mixture, which was fired onto the Lucalox. The Nb-1Zr was then brazed with the Ni/Nb/Ti brazing alloy. Photomicrographs of the resultant joints show that nearly all the yttria has migrated out of the originally porous tungsten structure and that the brazing alloy, or certain elements contained in it, filled the resulting voids in the tungsten. There is some indication that the brazing alloy also penetrated the Nb-1Zr substrate for a short distance, in the order of 0.001 to 0.002 inch, primarily along the grain boundaries. At the same time or shortly afterwards, there appears to have been a reaction

between the residual brazing alloy and the yttria which had migrated to the surface of the tungsten to form a complex glass, or mixture of glasses. This glassy layer then appears to have penetrated the grain boundaries of the Nb-1Zr in the wake of the brazing alloy, in such a way as to form a nearly continuous layer between the metallizing and the Nb-1Zr. It also seems from the sinuous shape of the Lucalox/tungsten interface that the tungsten/yttria metallizing sinter conformed to the surface of the Lucalox, eroding it into a series of small depressions. These depressions do not appear to be associated with the grain boundaries of the Lucalox (See Figure 19). Therefore the metal-ceramic seal consists of a series of interlocking or dovetailing layers which form a seal of exceptional integrity and strength.

In addition there is evidence of diffusion, probably of oxygen, from the glass layer into the Nb-1Zr substrate. The diffusion of the brazing alloy and the constituents of the yttria into the tungsten

metallizing caused delta-shaped "islands", grain boundary networks, and possibly a fine precipitate within the tungsten grains. A few roughly spherical "islands" of yttria also remain trapped within the tungsten layer.

The layer of glass in some places appears to consist of several phases.

The structure of the seal shows an excessive amount of glass. Since this seal was only examined after 2400 test hours at 1800°F, it is not possible to determine the cause and extent of the diffusion of the different phases. Diffusion of some kind could have taken place during either the metallizing, the brazing operation, or the life test.

Explanation of the structure is rather difficult in view of the fact that much of the diffusion mechanism consisted of a liquid or viscous phase percolating through a porous structure, and infiltration in the opposite direction by a liquid alloy.

In all the sections of this seal examined, no evidence was observed of cracking, separation, peeling or exfoliation of any of the layers comprising the seal. Most noteworthy are the sections illustrated in Figures 16 and 17 which show the border of the metallizing at the inner face of the Lucalox rings. The metallizing at these borders was subjected to the most severe stress, so much so that the Nb-1Zr blank end disc bulged under the test pressure without causing the metallizing to peel or crack.

#### 4.2 X-Ray Microprobe Analysis

An X-ray microprobe analysis was performed on a section selected to give optimum analysis of the phases observed in the photomicrographs. The trace traverse corresponds to the vertical line shown on Figure 19 running from Lucalox to Nb-1Zr. The traces given in Figures 20 to 22 have been displayed so that the right hand side of the trace corresponds to the top of the line indicated in Figure 19.



The elements analyzed for were W, Nb, Ni, Al, Y, and Ti. An accelerating potential of either 25 or 30 kilovolts was used. With a carbon-covered specimen, the current was 0.05 microampere. The variations in analysis across the section were recorded continuously, with marker pulses being recorded at 20 micron intervals.

The trace in Figure 20 was recorded using a lithium fluoride crystal at 25 kilovolts accelerating potential. The traces shown in Figures 21 and 22 were recorded using an ADP (ammonium di-hydrogen phosphate) crystal with a 4" radius at 30 kilovolts accelerating potential.

A negative print from a photomicrograph representing the same area traversed by the beam is shown in each figure, the photographs being lined up as closely as possible with the microprobe trace. The upper edge of the print represents the line actually traversed. An exact match was not feasible since the traces and photograph had to be enlarged or reduced for reproduction. The portions of the microprobe traces shown

at the right hand side of each trace will be discussed in greater detail as they represent the start of the traverse which appears in Figure 19. The opposite ends of the traces are similar in form but not identical, and do not appear in Figure 19.

Each trace is indexed with a line marked "edge", which represents the interface between the Lucalox and the metallizing, also a "background level" for the element being analyzed. The height of the trace above the "background level" indicates the relative amount of the element present. The marker pulses were masked off during reproduction of the traces, but each major division of the trace represents 20 microns, or 5 major divisions represent approximately 0.004 inch.

In some places where the material is known to be of essentially constant composition, e.g., in the center of the Nb-1Zr member, some peaks and valleys are observed. These are not peaks representing a change in composition, but are topographic features caused by discontinuities in the surface such as pits, grain boundaries, etc.

The traces of the different layers comprising the seal will be discussed separately in the following paragraphs.

a. Lucalox Layer

It is seen from all 6 traces that there is a sharp demarcation between the Lucalox and the metallizing. Except for a small Ti peak, which is probably topographic, there is no evidence of diffusion of any of the elements investigated into the Lucalox beyond the metal/Lucalox interface, although the photomicrograph shows irregular attack of the Lucalox by the metallizing.

b. Tungsten Metallizing Layer

The traces show the major elements present are W, Nb, and Ni. There is a remarkable similarity in the shapes of the W, Nb, and Ni traces which suggest an alloy of essentially uniform composition, i.e., a solid solution. Two sharp Al and Y peaks are present which presumably could represent the two rounded particles of glass observed in the photomicrograph of the tungsten layer (see Figure 19). Ti is present in small quantities.

c. Glass Layer

This layer, which is the major component of the reaction zone, appears to be composed of a high proportion of aluminum oxide, since the peaks are quite high in comparison to the Lucalox peak, which represents essentially pure  $\text{Al}_2\text{O}_3$ . Steep peaks are also present for Nb, Ti, Ni, and Y indicating that these elements are localized in the glass area in a non-uniform manner.

d. Nb-1Zr Layer

Although a penetration zone can be seen between the glass layer and the Nb-1Zr in the photomicrographs, the microprobe traces do not indicate diffusion of any of the elements analyzed from the glass layer into the Nb-1Zr.

The penetration zone might be caused by the penetration of oxygen into the Nb-1Zr.

A large number of test melts have been made where Ni/Nb/Ti alloys have been melted in small crucibles

of Nb-1Zr alloy. In each case, metallographic examination showed that the molten alloys had attacked the Nb-1Zr crucible with little or no evidence of intergranular attack.

However, the photomicrographs presented in this report indicate that the Nb-1Zr substrate has been attacked primarily in an intercrystalline manner by the glass formed in the metallizing operation.

It would appear that the presence of the oxygen exerted a marked effect on the ability of the Ni/Nb/Ti alloy to attack the Nb-1Zr substrate. It is felt that the Nb-1Zr substrate was attacked by oxygen, primarily along the grain boundaries, and that the Ni/Nb/Ti alloy then attacked the substrate, following the oxygen-rich paths provided by the grain boundaries. The result was to produce intergranular penetration of the substrate for a short distance by the glassy phase. This penetration was not of such an extent to be harmful but served to bind the layers together.

## 5.0 Compatibility Test Program

During the report period, potassium compatibility testing was completed on the four single convolution test capsules of C-129Y, FS-85, T-222 and W-25Re alloy and the one test capsule containing four representative electrical terminals. The test consisted of five 100-hour cycles at 1800°F (about 80 psia potassium vapor pressure). No potassium leakage was observed during the test. Examination of the test capsules after completion of the test showed no visible signs of failure.

The potassium was removed from the test capsules inside a vacuum purged ( $10^{-5}$  torr) welding chamber back-filled with high-purity helium. The tops of the test capsules were cut off and the capsules were heated to 150-200°F. The potassium was drained from each test capsule into a platinum dish and, upon removal from the chamber, converted to KC .

To remove the residual potassium from the test capsules, the drained capsules were sealed inside a stainless steel distillation chamber. The distillation

chamber was removed from the welding chamber and evacuated to  $10^{-5}$  torr. The bottom half of the distillation chamber was heated to 800°F and the residual potassium was collected on an air-cooled finger at the top of the distillation chamber. The test capsules were heated in this manner for 72 hours, during which time the pressure remained at about  $10^{-5}$  torr.

Upon removal from the distillation chamber, all five test capsules were found to be coated externally with a dark gray film. Much of this dark film appeared to be water-soluble and was probably caused by condensation of potassium vapor during the distillation process.

#### 5.1 Examination of the Test Capsules

The test capsule containing the electrical terminals was opened first. This was done by machining off the weld bead around the rim, extracting the terminals, and then sectioning both the capsule and the upper tube by sawing them longitudinally.

The four pressure compatibility capsules were next sectioned by removing the capsules from the upper tube, and then sectioning the pressure capsules with a water-cooled cut-off wheel. The upper tubes were sectioned longitudinally by sawing with a band saw.

The longitudinal sections of the four pressure compatibility capsules appeared bright and clean, with little or no evidence of any attack by the potassium, whereas the inside of the capsule containing the terminals was blackened somewhat. When the vertical tubes of the pressure compatibility capsules were sectioned, they were also found to be slightly blackened. It appears likely that the black film existed inside the pressure capsules; but being water-soluble, the film was removed by the cooling water used with the cut-off wheel.

Figures 23 to 27 show photographs of the five test capsules in the "as sectioned" condition. Figure 23 shows the terminal capsule with one terminal in



position, the other three terminals having been removed. It is seen that while the lower part of each terminal cavity is bright and clean, the housing shows traces of a white corrosion product where the Lucalox portion of the terminal was in contact with the housing. The upper tube shows a black corrosion product along its length.

Figures 24 to 27 show the pressure compatibility capsules after sectioning. It is seen that in each case the lower portions of the pressure capsules are clean and almost free of corrosion while the upper portions show small amounts of a black corrosion product. As described above, this black coating could have been removed in some cases during sectioning the capsules with a water-cooled cut-off wheel. In the C-129Y capsule (Figure 24) and the FS-85 capsule (Figure 25), the boss in the center of the lower diaphragm was found to be pressure-welded to the limiting stop after the test at 1800°F.

The capsule containing the electrical terminals was examined immediately after sectioning longitudinally,

and then photographed (see Figure 23). The lower part of the capsule containing the electrical terminals was photographed at a higher magnification. (See Figure 28). Figure 28 shows that only the upper part of each cavity, which contained one terminal, was coated on the inside in varying degrees with a white incrustation of a salt-like material, probably a potassium oxide, hydroxide or carbonate.

Both the Lucalox and metal parts of the terminals showed a frosted or etched appearance compared with the "as received" terminals. Each one of the four terminals tested showed longitudinal and radial cracks in the outer band of Lucalox. (See Figure 25, Reference 2)

The four terminals were then opened by machining off the FS-85 caps on the lower ends of the terminals. Photographs of the terminals in this condition are shown in Figure 29. Two of the terminals when opened were found to contain the white potassium compound observed on the outside of the terminals. All four

terminals were then helium leak tested; three were found to be leak-tight and one to have a leak. Of the three units that were found to be leak-tight, one was filled with the white potassium compound. Apparently, the electron-beam weld joining the small cap to the terminal leaked, because the potassium compound was only present in the very bottom of the terminal. Thus, it appears that three out of the four terminals were leak-tight after the test, even though the outer band of Lucalox was cracked.

The pressure capsules were mounted in plastic, polished with emery strips and fine diamond paste. They were then polished by alternately etching in "mixed acids" (equal parts HF, H<sub>2</sub>SO<sub>4</sub> and HNO<sub>3</sub>, diluted 1:1 with water) and hand polishing on a wheel charged with fine alumina and moistened with 4% ammonium bi-fluoride solution. In each case the FS-85 housing around the capsules (or the molybdenum yoke around the W-25Re capsule) was removed by sawing prior to mounting. The yokes which had been welded across the bottom of

the housings to limit the deflection of the capsules were found to be pressure welded to the small bosses projecting from the centers of the lower diaphragms in the case of the C-129Y and FS-85 capsules. This did not occur in the T-222 and W-25Re capsules.

Examination of the cross-sections of all the pressure capsules at up to 400 X magnification showed no evidence of attack at the inside of the capsules by the potassium. The only abnormal feature found was that the capsule boss was pressure welded to the yokes as described above. In addition, an intergranular crack was observed in the outer surface of the T-222 capsule. This intergranular crack originated in the radius of the internal corner between the central boss of the lower diaphragm and the diaphragm proper, and extended inwards at a 45° angle approximately one-third of the way through the diaphragm. (See Figure 38). Apparently a machining fault provided a stress concentrating notch in the vicinity of the boss, causing the crack.

Photographs of the pressure capsules at 3X magnification are shown in Figures 30 to 33. These figures

show the general arrangement of the parts in the pressure capsules and the welds.

The pressure capsules were next photographed at 25X magnification. In each case the area photographed comprised a section of the weld joining the diaphragm material to the tube, and also a portion of the lower diaphragm opposite the weld. It is seen that in each case (Figures 34 to 37 ) there is no evidence of attack of either the diaphragm material, the tube, or the weld nugget, which was composed of an alloy of the tube and diaphragm materials. In the case of the C-129Y, FS-85 and T-222 capsules the tube was FS-85, and in the case of the W-25Re capsule it was Mo-50Re.

Figure 38 shows the intergranular crack in the T-222 capsule diaphragm.

## 5.2 Potassium Analysis

The potassium was analyzed before and after the compatibility tests. The assay results are summarized in Table 3 where the left hand column shows the chemical analysis of the potassium at the start of the

TABLE NO. 3

Potassium Analysis Before and After Compatibility Test.  
(Test run for 500 hours at 1800°F and nominal 80 psia pressure)

Element	After Test (ppm)					
	Before Test (ppm)	C-129Y	FS-85	T-222	W-25Re	Terminal Capsule
Ag	<1	<1	<1	<1	<1	<1
Al	<1	1	<1	1	1	1
Be	-	<1	<1	<1	<1	<1
Ca	1	1	<1	10	1	10
Cb	<1	10	<1	<1	<1	<1
Co	<1	<1	<1	<1	<1	<1
Cr	<1	<1	<1	<1	1	1
Cu	<1	<1	<1	<1	<1	<1
Fe	<1	1	<1	1	5	5
Mg	<1	<1	<1	<1	<1	1
Mn	<1	<1	<1	<1	<1	<1
Mo	<1	<1	<1	<1	>25	<1
Na	5	10	5	<10	10	10
Ni	<1	1	<1	<1	1	<1
Pb	<1	<5	<5	<5	<5	<5
Si	5	<10	<5	<10	<10	<15
Sn	<1	<5	<5	<5	<5	<5
Ti	<1	<1	<1	<1	1	<1
V	<5	<10	<5	<10	<10	<10
Zr	<1	<5	<5	<5	<5	<5
O	3.4 - 7.6*	-	-	-	-	-

\* O as K<sub>2</sub>O

test, and the other columns show the chemical analysis of the potassium extracted from the test capsules after the test.

The Na assays of the potassium in each case showed some variation during the test, but this is not thought to be significant.

With the exception of the FS-85 capsule, in each case the V content of the potassium increased during the test. The spectrographic analysis of V is apparently not particularly sensitive, so some doubt must be cast on the results, but the trend of the results suggests that V was leached out of these alloys during the test.

In all cases, the changes in potassium analysis are sufficiently small to indicate material compatibility.

Oxygen analysis was only performed on the potassium at the start of the test, and was reported as 3.4 to 7.6 ppm (as K<sub>2</sub>O), the analysis being performed by the mercury amalgamation method under a helium cover.

The most significant changes in the potassium analyses in each test capsule were as follows.

- a. C-129Y Capsule. The most significant change was an increase in Cb content of the potassium from <1 to 10 ppm. This Cb presumably was leached out of the C-129Y and not out of the FS-85 parts of the capsule, since no Cb was leached out of any of the other capsules containing FS-85 parts. This attack might have been a differential corrosion effect.

Increases in Al, Fe, Ni, Pb, Si, Sn, V and Zr contents were also reported, but are not considered to be significant.

- b. FS-85 Capsule. The potassium from this capsule showed the least change in composition during the test. The only increase in impurities observed were in the Sn and Zr contents of the potassium.

The Si content showed a slight decrease. This exceptional stability may be due to the fact that the capsule was fabricated entirely of FS-85 material, in contradistinction to all the other capsules which contained dissimilar materials.



- c. T-222 Capsule. In this capsule a marked increase was observed in the Ca content of the potassium from  $<1$  to 10 ppm. No explanation can be offered for this.

Increases in Al, Fe, Pb, Si, Sn, V and Zr were also reported but are considered insignificant.

- d. W-25Re Capsule. The most marked change was the relatively large increase in Mo content of the potassium from  $<1$  to  $>25$  ppm. In view of the fact that Mo is normally considered to be quite resistant to potassium this attack, which is considered to be abnormally severe, is probably due to some preferential corrosion effect as a result of W-25Re, Mo-50Re and TZM molybdenum being in contact in the capsule.

Increases were found in the Al, Fe, Pb, Si, Sn, Ti, V and Zr contents of the potassium, but of these only the increase in Fe is considered to be significant.

e. Terminal Capsule. In this capsule the major changes in impurities in the potassium were increases in the Ca, Fe and Si contents, accompanied by minor increases in the Al, Cr, Mg and V contents.

The following analysis has been obtained of the impurities in a sample of Lucalox.

MgO	1000 ppm
Fe <sub>2</sub> O <sub>3</sub>	100 ppm
SiO <sub>2</sub>	300 ppm
CaO	100 ppm
CuO	Trace
NiO	Trace
MnO	Trace
Cr <sub>2</sub> O <sub>3</sub>	Trace

While not necessarily indicative of the average impurity level of the test terminals, it is seen that with the exception of V, all the impurities which increased during the test could have been present initially in the Lucalox, indicating that the Lucalox was the probable source of the additional potassium impurities.

## 6.0 Transducer Signal Conditioning

During the report period, the various functional blocks of the transducer signal conditioning system were established. To facilitate initial loop testing of the transducer, the electrical conditioning system will be set up to operate on 110 volts, 60 cps input power. Provisions can be made for operation from other power sources (e.g., 28 volts dc, 28 volts 400 cps, 28 volts 1000 cps) which are common in the aerospace field. Figure 39 presents the electrical conditioning system in block diagram form.

The conditioning system includes four control loops:

1. a secondary reference collector loop,
2. a heater control loop,
3. a thermionic diode sensor control loop and
4. a resistance thermometer loop.

The secondary reference collector and heater control loops are functionally tied together in that the secondary reference collector which is embedded in, and electrically isolated from, the reference

collector, senses the emission capability of the emitter. If the emission falls to a value sufficiently small to cause the thermionic diode to become emission limited, the heater control loop supplies more power to the transducer heater, thereby raising the emitter temperature to the point where the thermionic diode again becomes space charge limited. To avoid excessive current surges in the heater, a constant current regulator with internal reference controls the current to the transducer heater. A voltage regulator supplies the secondary reference collector potential. The secondary reference collector programs a feedback current from the magnetic amplifier to stabilize the heater control loop at the desired emitter temperature (2100°F).

The thermionic diode sensor control loop provides the constant sum-of-the-currents function through a constant current regulator which is adjustable to any value between 100 and 300 milliamperes. The difference current is derived from low ohmage

resistors inserted in the collector legs of the diode sensor. The voltage developed across the resistors is amplified by a low drift differential amplifier to deliver a 0-5 volt signal proportional to the input pressure.

The resistance thermometer loop uses a band of tungsten/yttria metallized on the thermionic diode Lucalox base to sense the temperature of the pressure capsule. The resistance change of the tungsten/yttria with temperature unbalances a bridge circuit and introduces a gain correction into the differential amplifier to compensate for the change in Young's modulus of the pressure capsule material.

Detailed design studies of the conditioning system are being performed to further define the various parameters and signal levels. An initial breadboard model of the system components is being fabricated.

## 7.0 Differential Pressure Transducer

During the report period, experimental work on the differential pressure transducer involved a mock-up of a mechanical configuration using a cantilever structure with combination end load and end couple reactions. This configuration is shown in Case III, Figure 40. Nb-1Zr tubing was used for both the outer and inner tubular beams of the mock-ups. Nb-1Zr was chosen for two reasons.

1. Nb-1Zr has a Youngs modulus about equal to that of the refractory alloys under consideration for use in the actual transducer.
2. Nb-1Zr tubing is readily available, in various sizes, for test purposes.

Three mock-ups were fabricated for testing. All used the Case III configuration of Figure 40. The first mock-up used a brazed assembly with an outer tubular beam of 0.187 inch O.D., 0.137 inch I.D. and an inner tubular beam of 0.096 inch O.D., 0.086 inch I.D.. Initial testing yielded erratic results. Investigation showed that the braze joint holding the outer

and inner beams together had failed and the inner beam had become loose. A second mock-up was made using the same size inner and outer beams but the assembly was welded together. Test results obtained from the second mock-up indicated that for an applied force of one pound, an inner beam deflection of about 0.0002 inch was obtained.

Further calculations indicated that an outer beam diameter of about 0.125 inch was required to obtain an inner beam deflection of 0.001 inch. Figure 41 shows plots of the theoretical deflection versus diameter relationship for each case of Figure 40. To generate Figure 41, it was assumed that (1) the outer beam was 1.5 inches long, (2) the inner beam extended 0.375 inch beyond the fixed support of the outer beam to form the active collector surface, (3) the force exerted by the pressure capsule on the beam was one pound, and (4) the Youngs modulus of the outer beam material was about  $30 \times 10^6$  psi. The equations for these relationships may be found in the Fifth Quarterly Report (Reference 1).

The third mock-up used a welded assembly with an outer tubular beam of 0.125 inch O.D., 0.075 inch I.D. and an inner tubular beam of 0.063 inch O.D. and 0.051 inch I.D.. The inner beam deflection was monitored by a Distance Meter capable of accurate measurement of distances from 50 microinches to 0.5 inch depending on the probe used. A probe is electrically connected to the instrument and brought into proximity with the flattened end of the inner beam (active collector surface). The capacitance formed between the probe and the inner beam is calibrated in terms of distance. The probe used had a full scale range of 0.005 inch with an accuracy of  $\pm 0.0001$  inch. A typical force versus deflection characteristic is shown in Figure 42. The data indicate that application of a one pound force resulted in an inner beam deflection of about 0.0007 inch. The force versus deflection curve is linear within 3 percent of full scale deflection corresponding to a one pound force. There appears to be no detectable hysteresis effect.



It was thought possible that low-frequency resonant effects could produce large scale beam motion. Therefore, the mock-up was installed on a vibration table and subjected to vibrations based on procedure XIV of MIL-E-5272C(ASG). The procedure involved the following test parameters.

0 to 10 cps,	0.20 inch double amplitude
10 to 20 cps,	$\pm 1.0g$
20 to 90 cps,	0.05 inch double amplitude
90 to 2000 cps,	$\pm 20g$

Prior to testing of the complete mock-up, the probe of the Distance Meter was vibrated by itself to check if the probe might exhibit any resonance at the frequencies of interest. The probe used for the vibration test had a full scale range of 0.010 inch with an accuracy of  $\pm 0.0002$  inch. The decreased accuracy of this probe was acceptable for this test since a qualitative idea of the resonant behavior of the beam was all that was desired. The probe exhibited no resonant points at the frequencies used for the test.

Results of the vibration tests of the beam in air showed that the Case III beam configuration had relatively broad resonant peaks between 220-250 cps, 700-820 cps, and 1400-1600 cps, and a sharply defined resonance at about 330 cps. Should these resonant peaks exist while the beam is in operation, the transducer output would be in considerable error. However, in operation the beam will be immersed in liquid metal, and therefore, subject to greatly increased damping conditions. For this reason, the resonant motion of the beam will be certainly minimized if not eliminated completely.

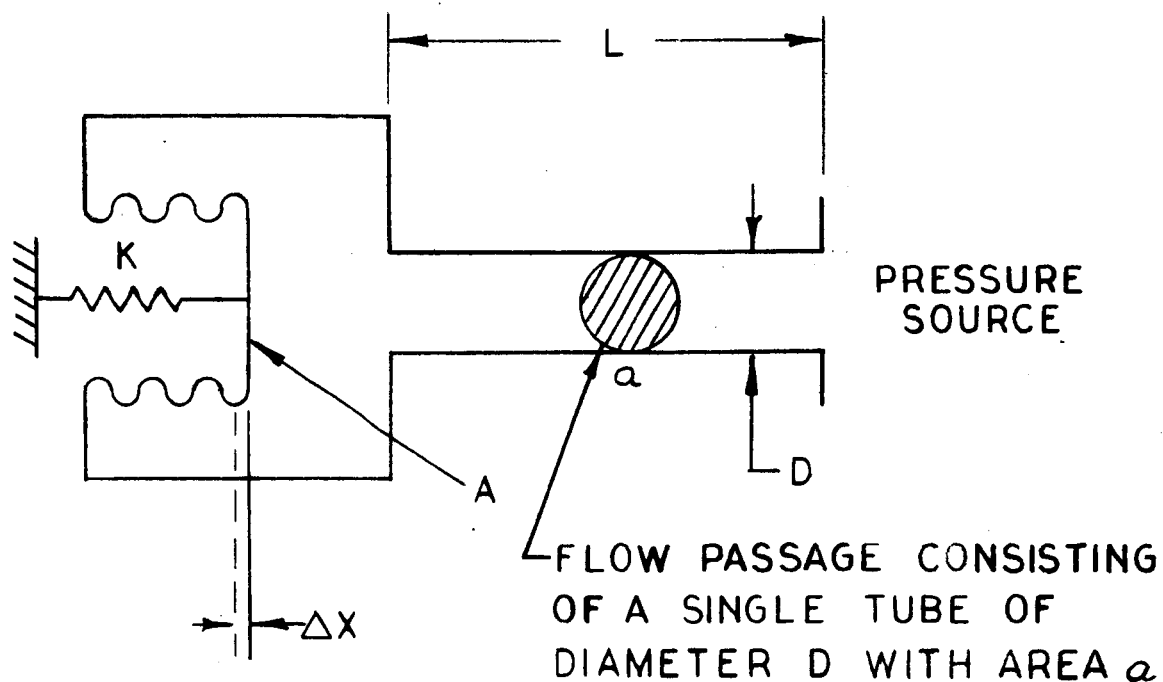


**FIGURE 1a**

**Basic Pressure Transducer System**

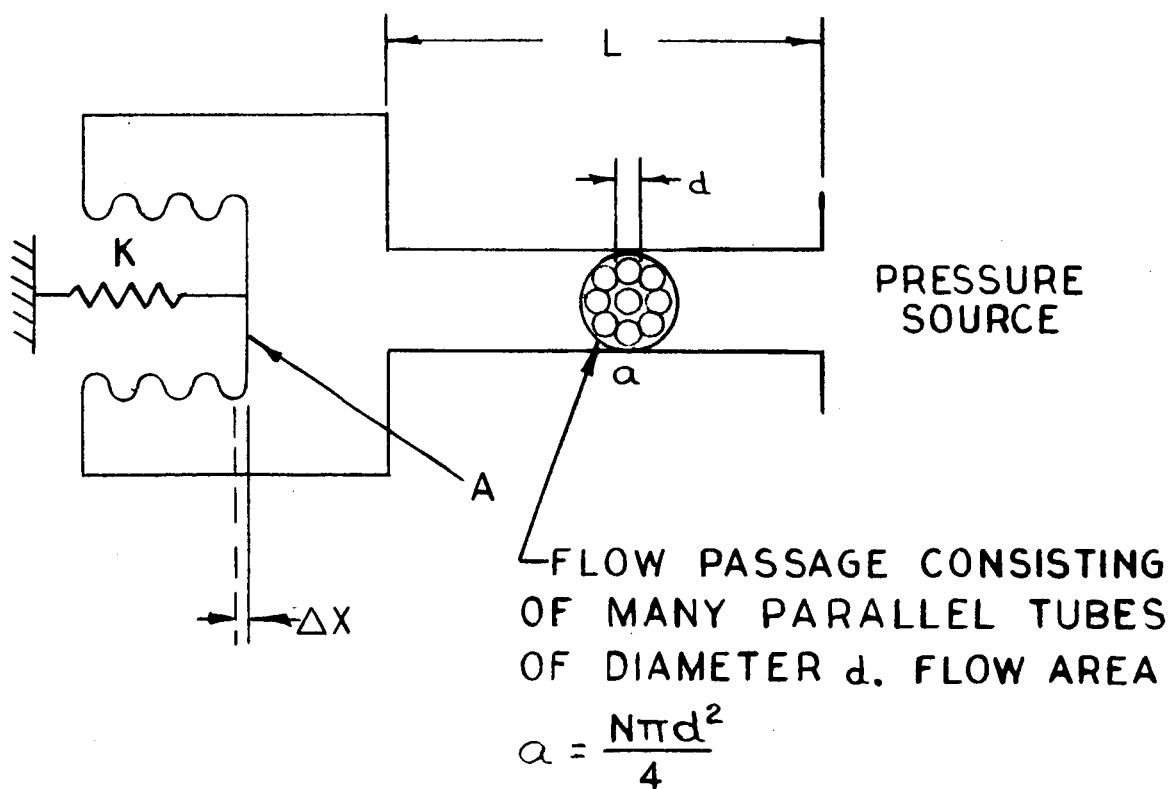


**FIGURE 1b**

**Pressure Transducer System with Snubber**

$$f_n = (23) \left( d \sqrt{\frac{N}{L}} \right) \left( \frac{1}{\sqrt{\rho}} \right)$$

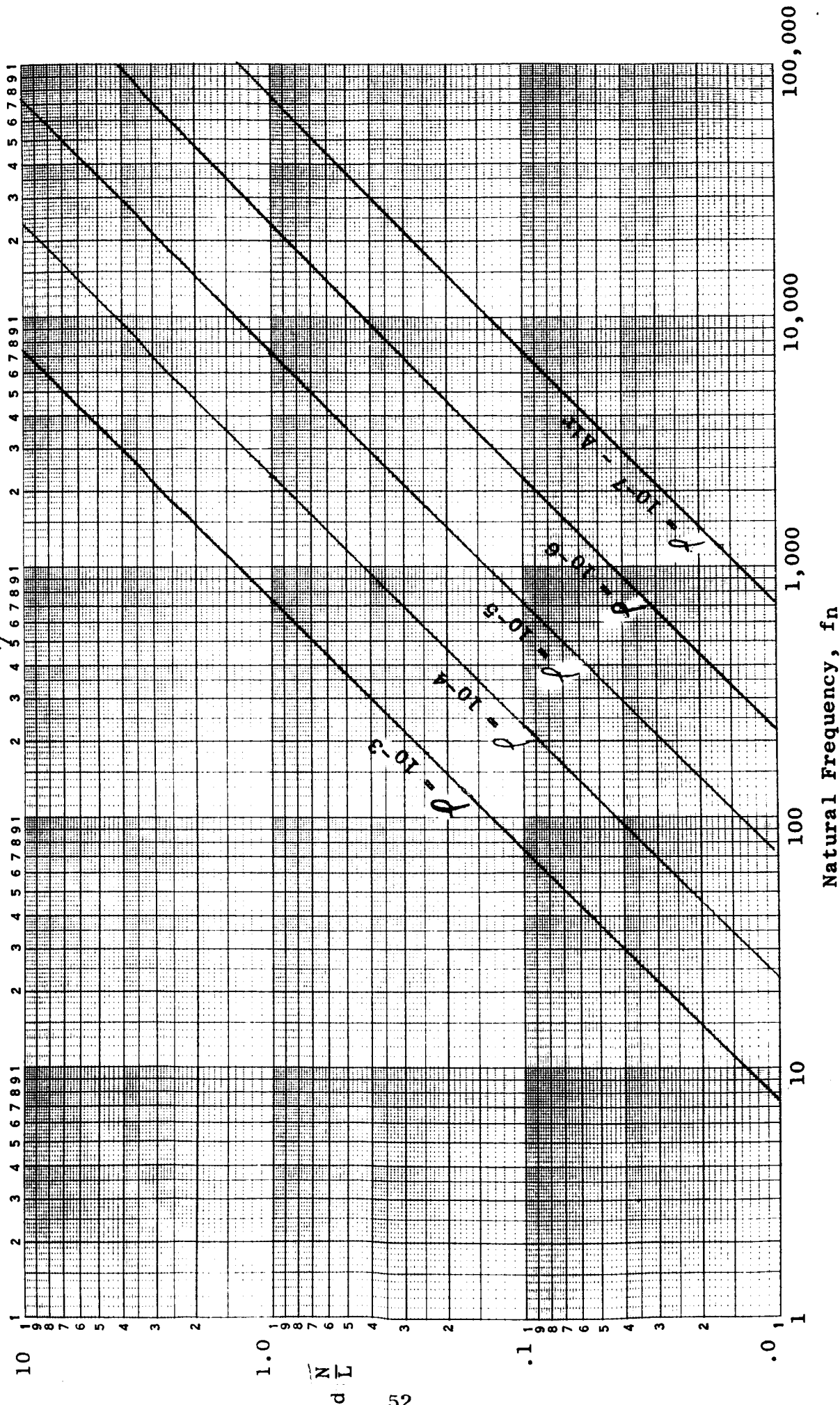


FIGURE 2  
Transducer Natural Frequency Characteristics

$$h = \left( 16 \sqrt{\frac{3}{\pi \Delta P}} \right) \left( \frac{\mu}{\sqrt{\rho}} \right) \left( \frac{1}{d^3} \sqrt{\frac{L}{N}} \right) = (83.4 \times 10^{-3}) \left( \frac{\mu}{\sqrt{\rho}} \right) \left( \frac{1}{d^3} \sqrt{\frac{L}{N}} \right)$$

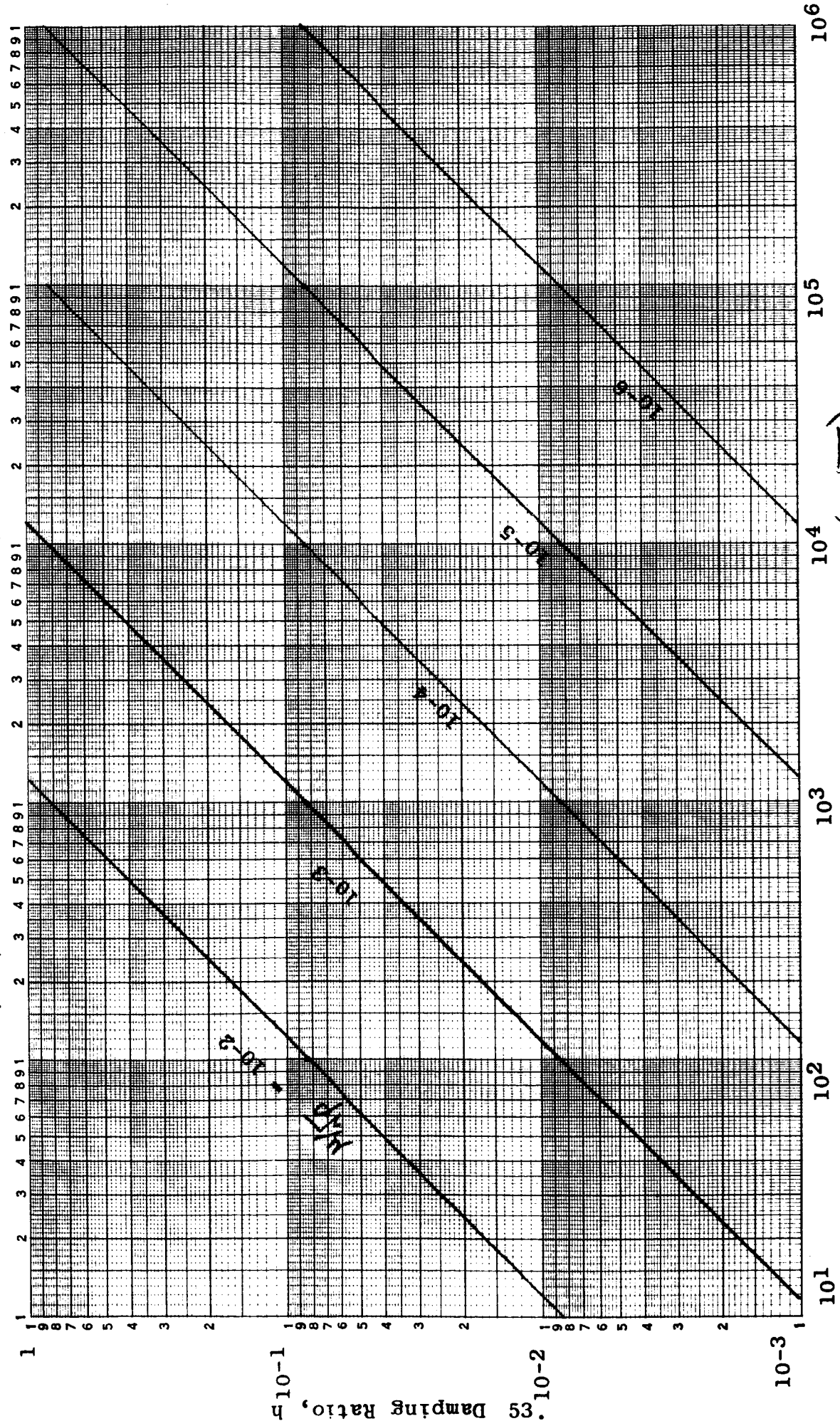


FIGURE 3  
Transducer Damping Characteristics

For Systems of the Type Where the  
Amplitude Ratio =

$$\frac{1}{\left[1 - \left(\frac{f}{f_n}\right)^2\right] + 2jh \frac{f}{f_n}}$$

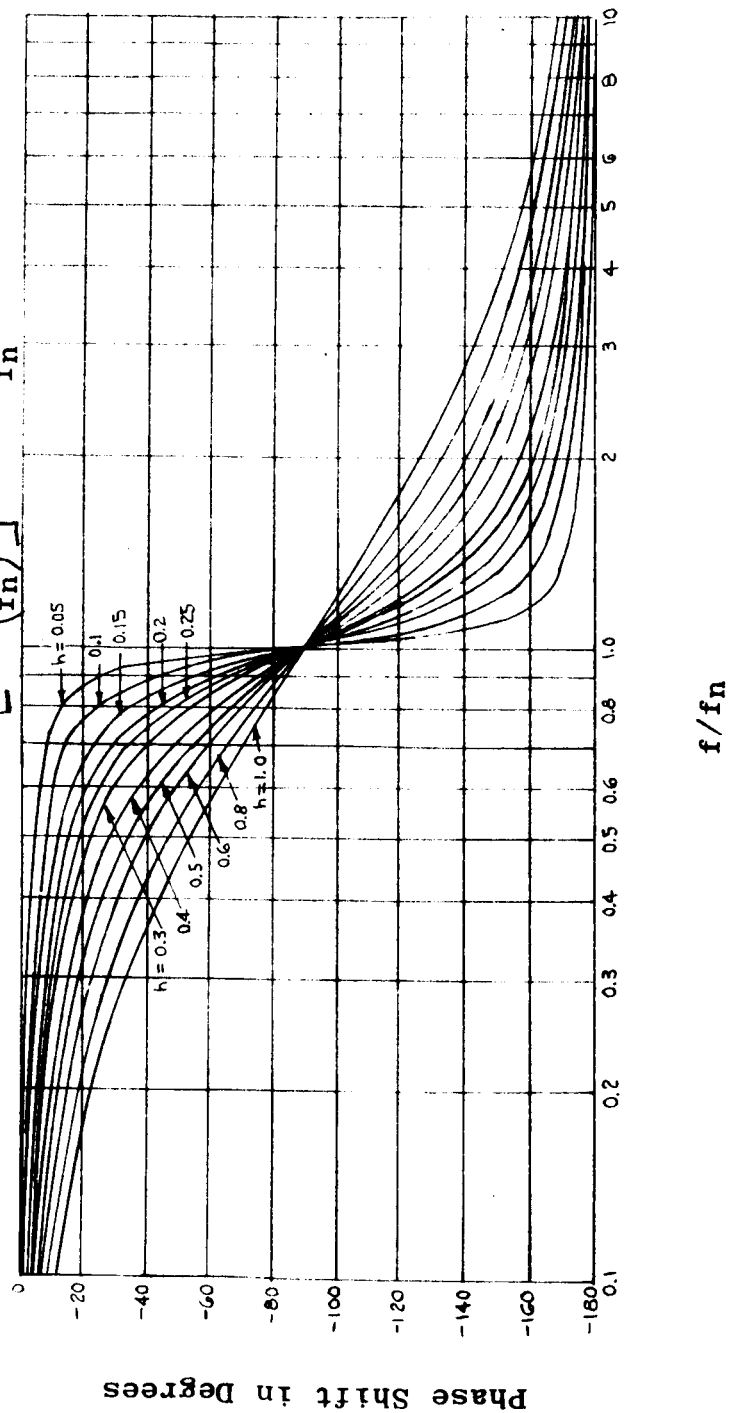


FIGURE 4

Transducer Phase Shift Characteristics

For Systems of the Type Where the  
Amplitude Ratio =  $\frac{1}{\left[1 - \left(\frac{f}{f_n}\right)^2\right] + 2jh \frac{f}{f_n}}$

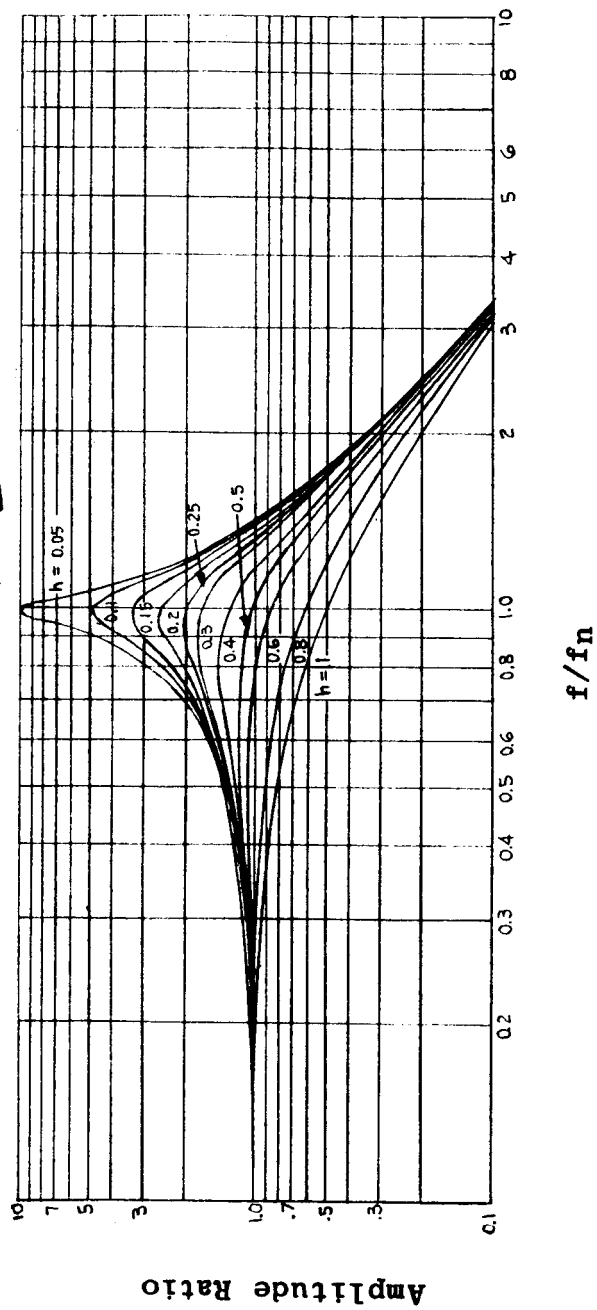


FIGURE 5  
Transducer Amplitude Ratio Characteristics

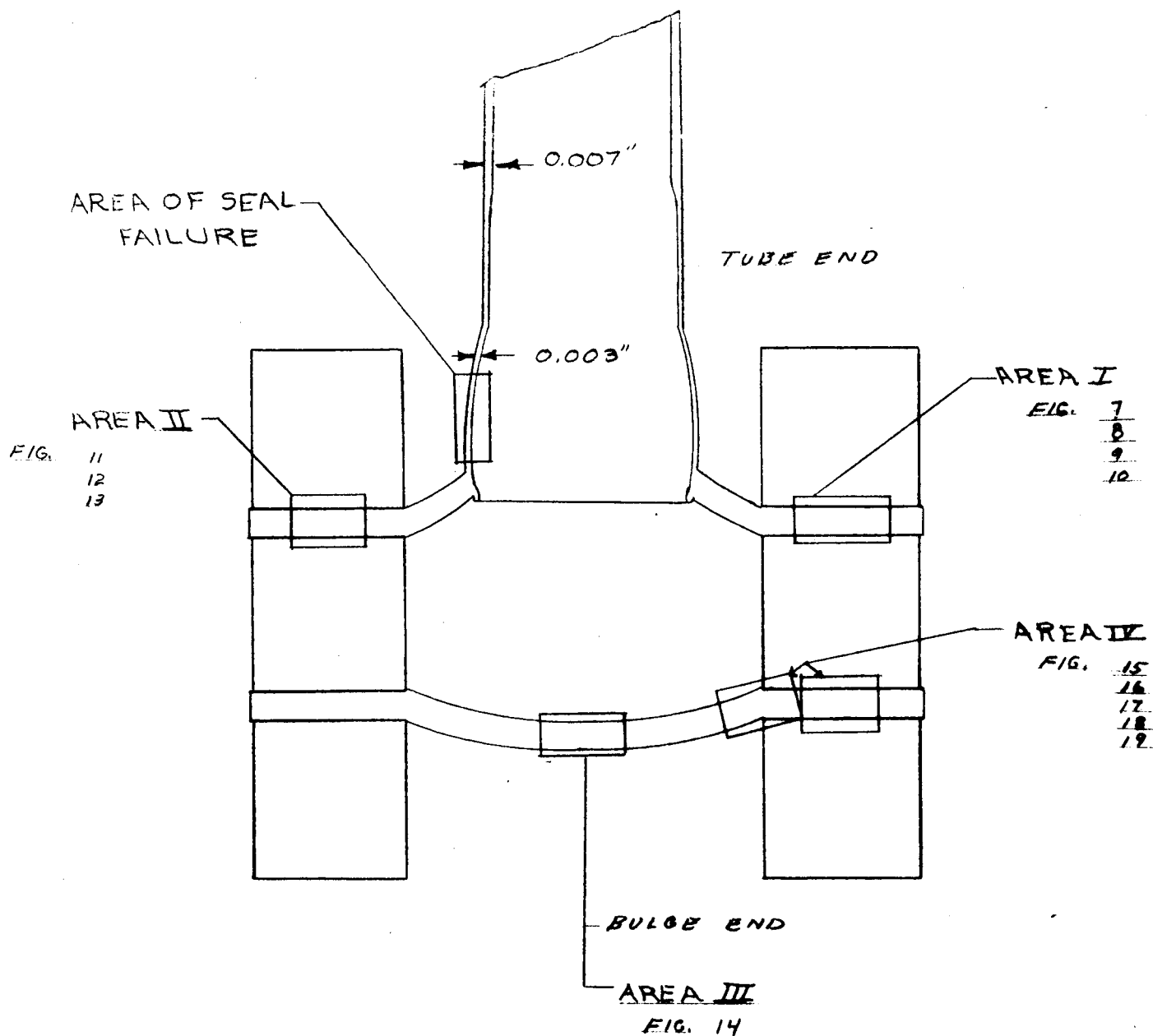


FIGURE 6  
REPRESENTATIVE Nb-1Zr/LUCALOX SEAL



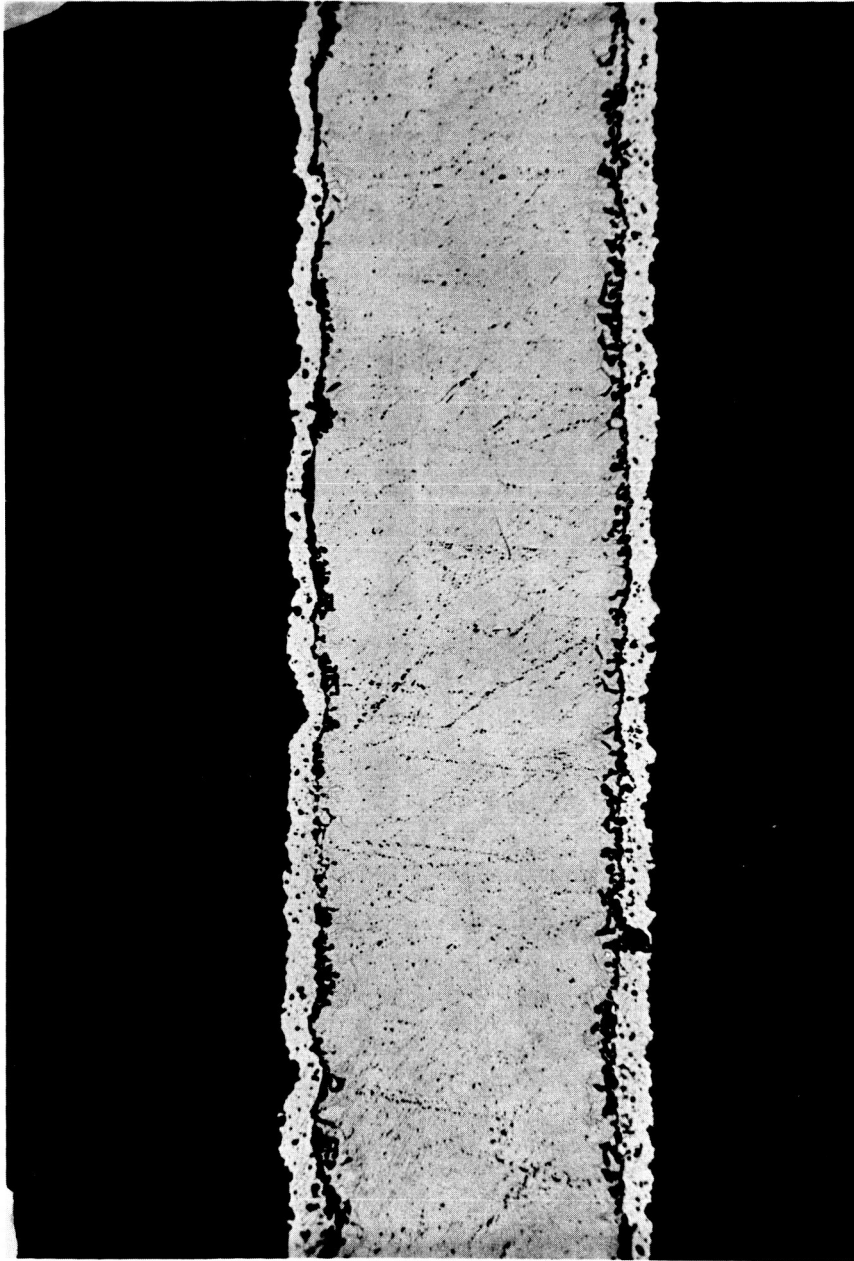


FIGURE 7

Ceramic to metal seal, tube end, unetched, 100X, Area I

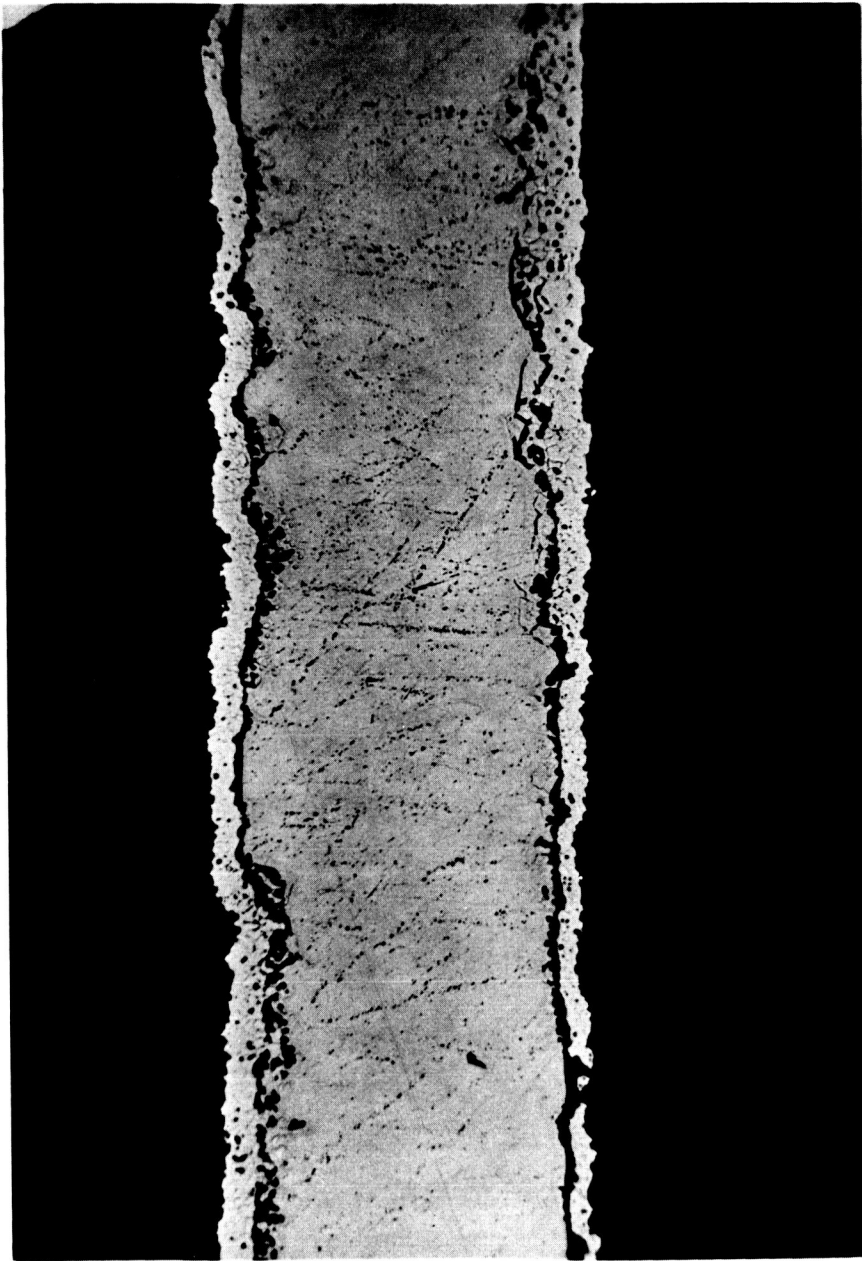


FIGURE 8

Ceramic to metal seal, tube end, unetched, 100X, Area I, site of  
Figures 9 and 10



FIGURE 9

Tube end interface showing glass, etched, 500X, Area I

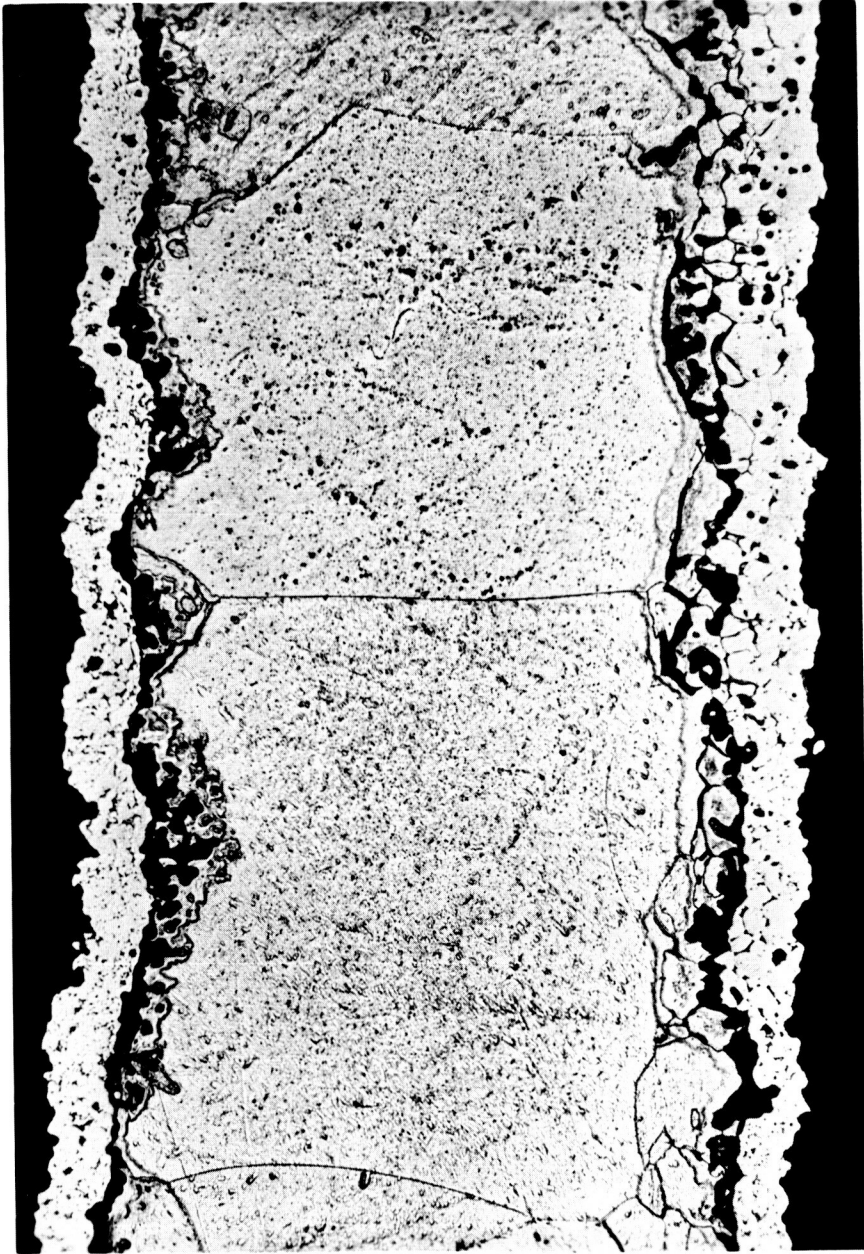


FIGURE 10

Tube end metal member showing large grain size, etched, 200X, Area I

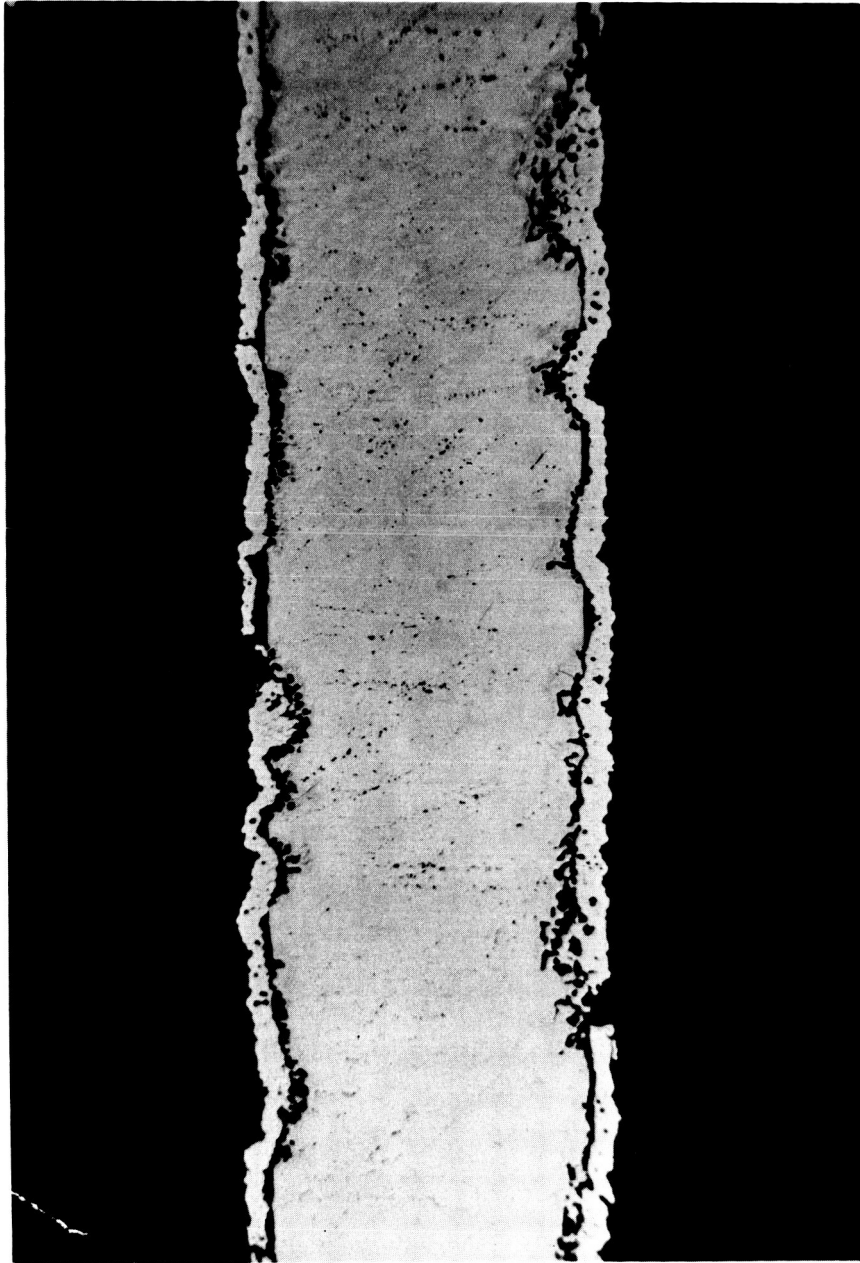


FIGURE 11

Ceramic to metal seal, tube end, unetched, 100X, Area II, site of Figures 12 and 13



FIGURE 12

Tube end metal member showing large grain size, etched, 200X, Area II



FIGURE 13

Tube end interface showing crystal-glass, oxygen attack, etched, 500X,  
Area II



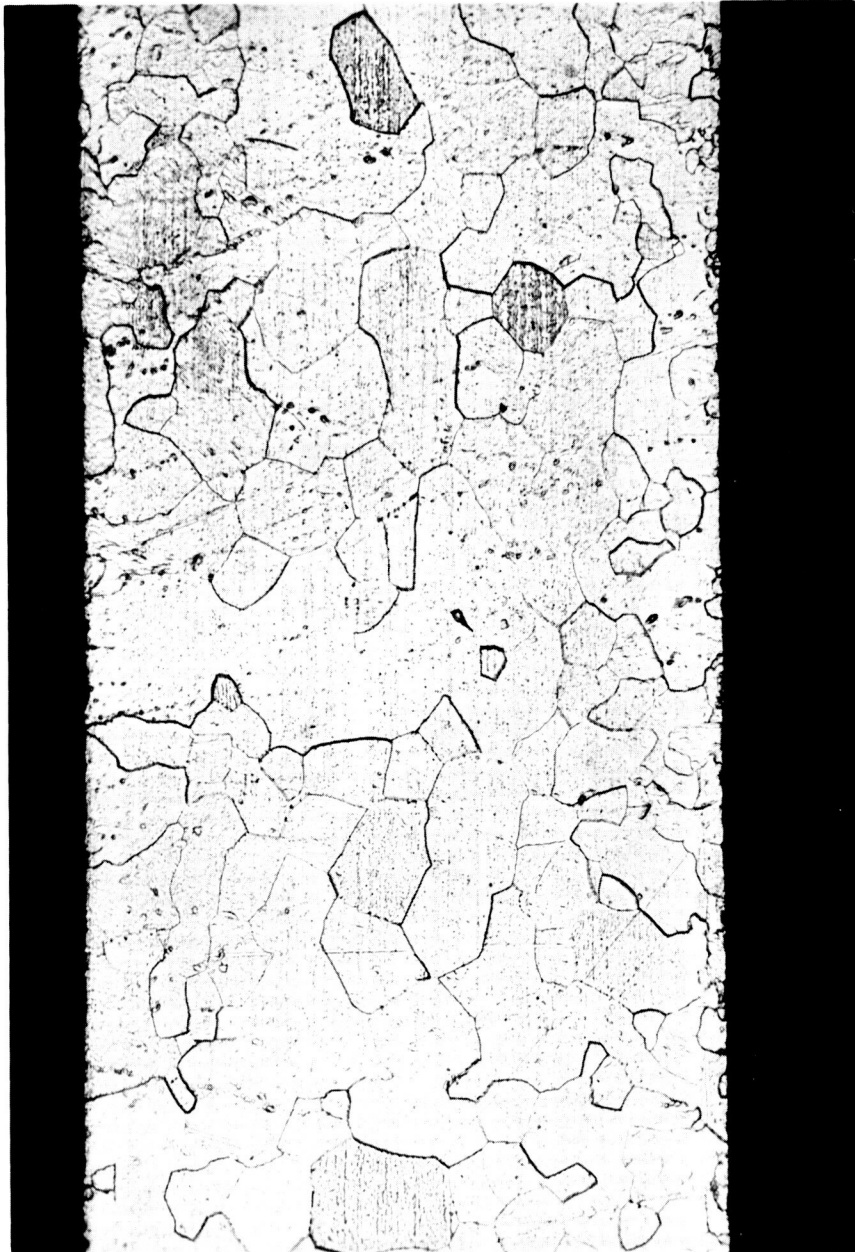


FIGURE 14

Bulged end, central portion of lower end plate, (Nb-1Zr), 200X,  
etched, Area III





FIGURE 15

Ceramic to metal seal, bulged end, unetched, 100X, Area IV, site of Figures 17 and 18. Section across which X-ray probe is taken.

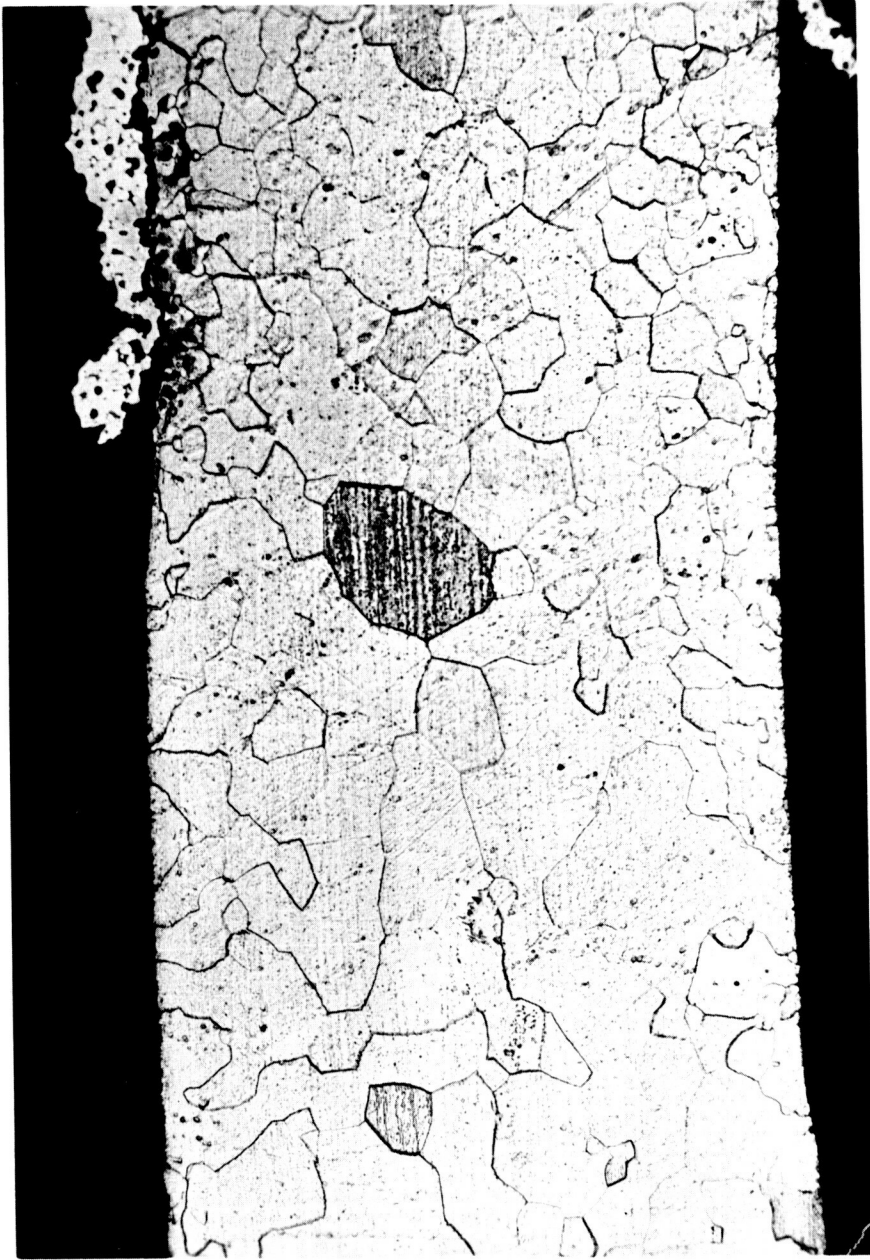


FIGURE 16

Bulged end metal member at braze meniscus area, etched, 200X, Area IV

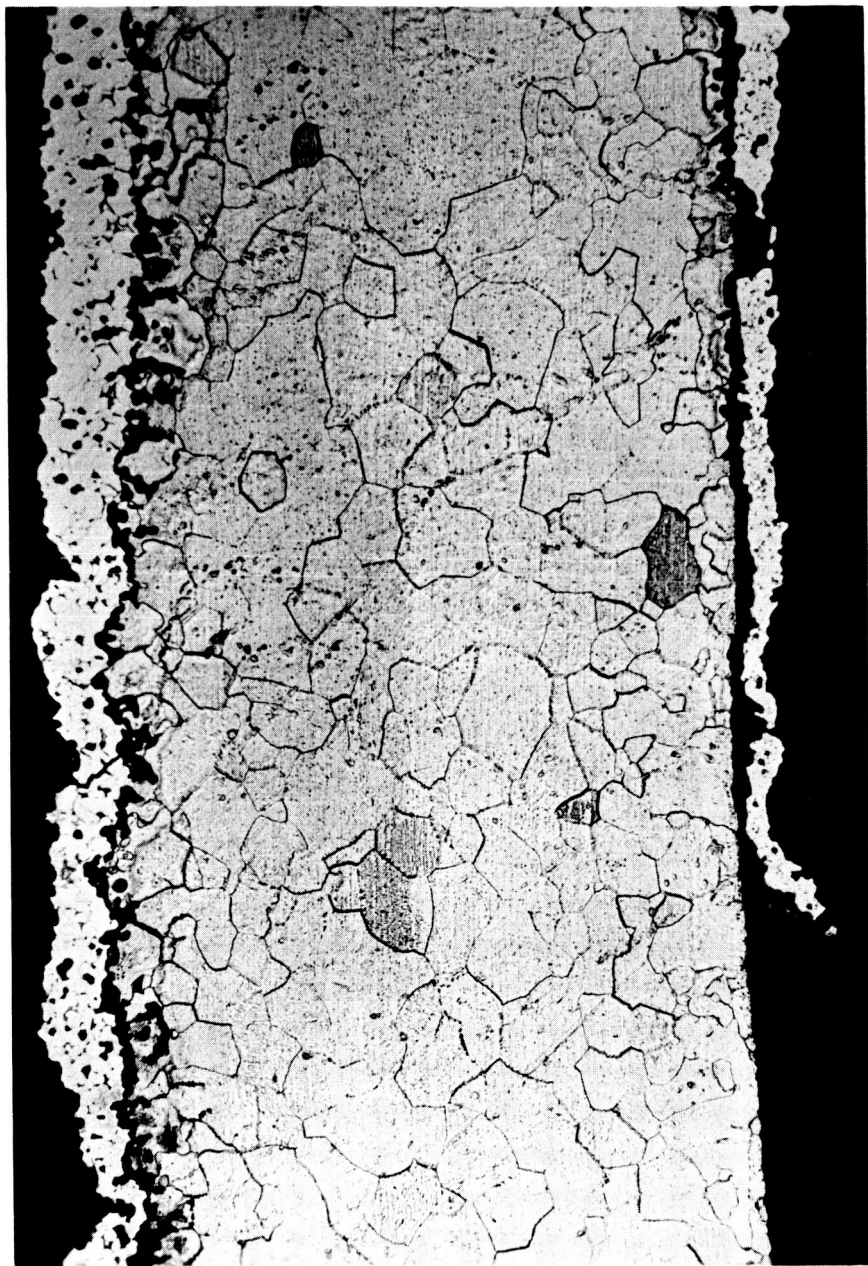


FIGURE 17

Bulged end metal member at braze meniscus area, etched, 200X, Area IV

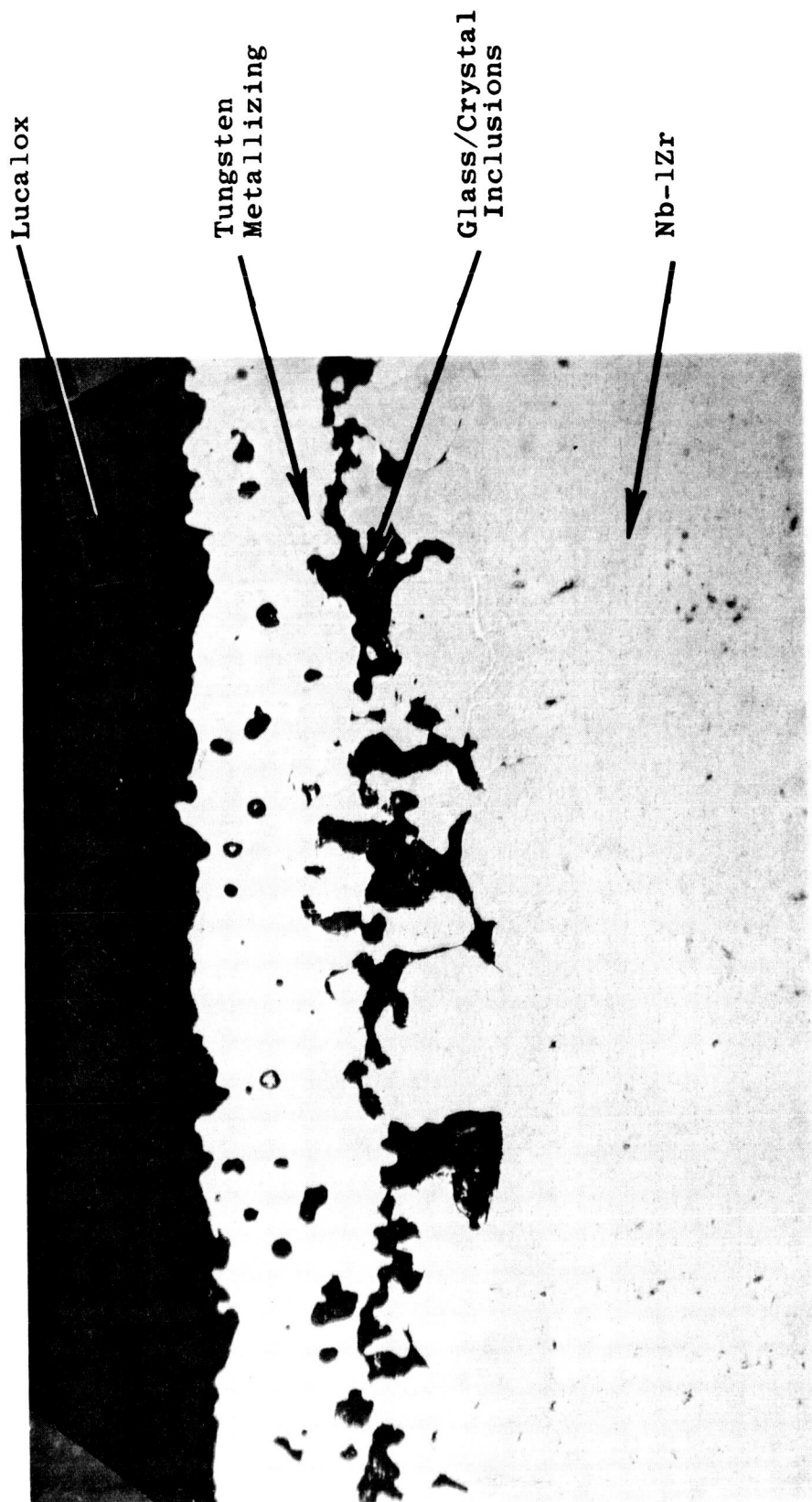


FIGURE 18

Bulged end interface showing crystal-glass, oxygen attack, etched, 500X, Area IV.

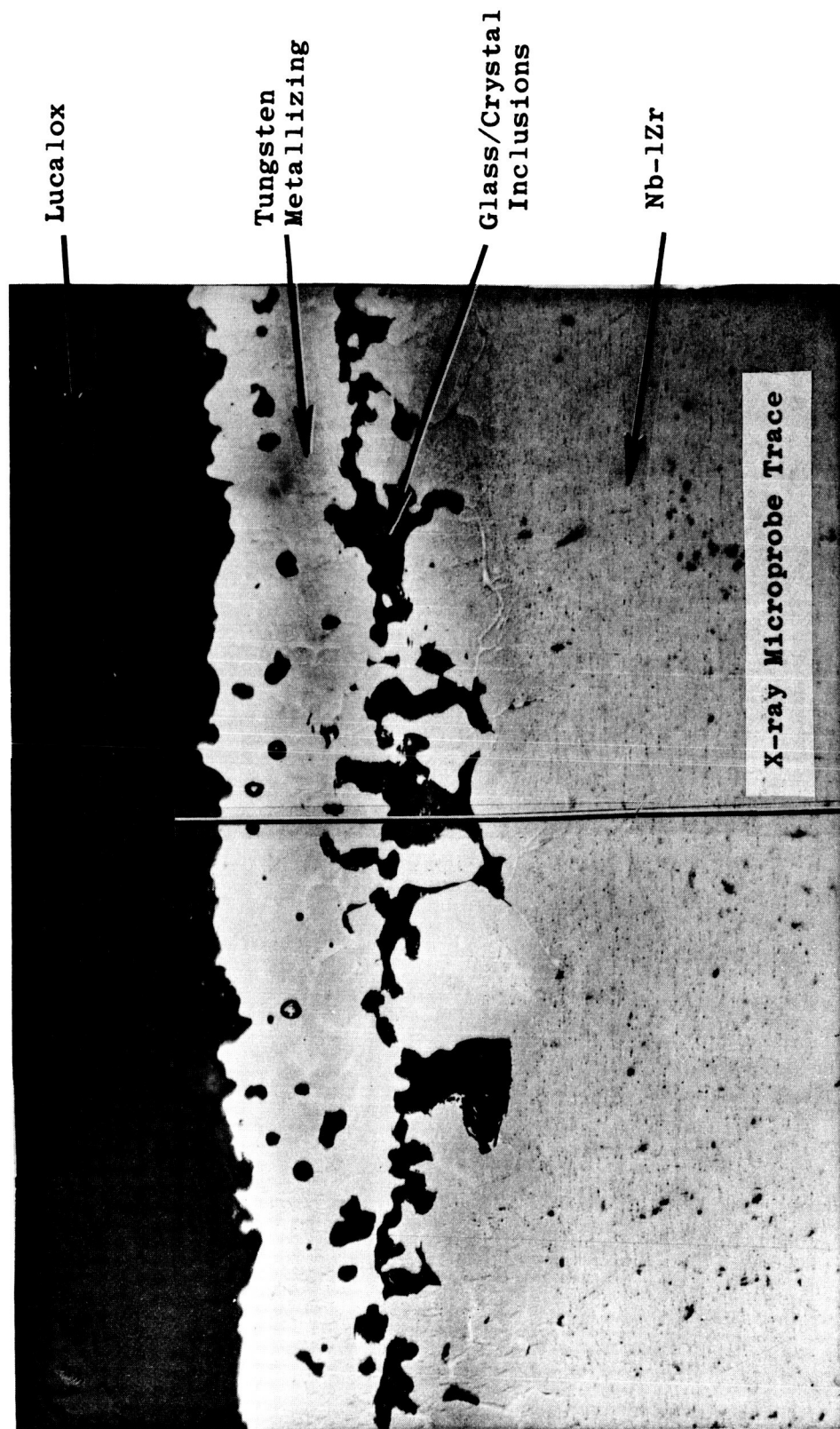
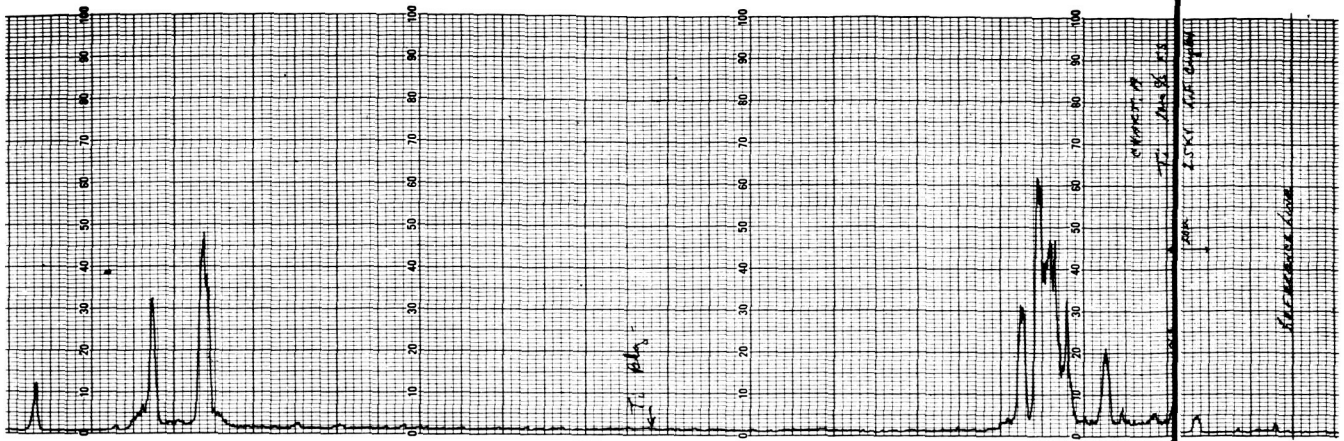


FIGURE 19

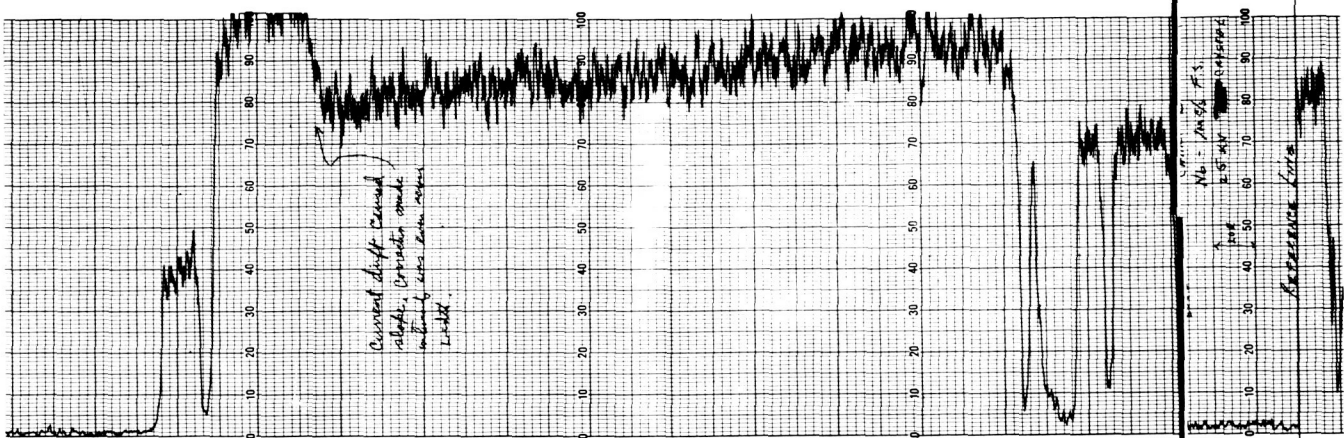
Bulged end interface showing crystal-glass, oxygen attack, etched, 500X, Area IV. Shows X-ray microprobe trace line.





Ti Trace

Edge

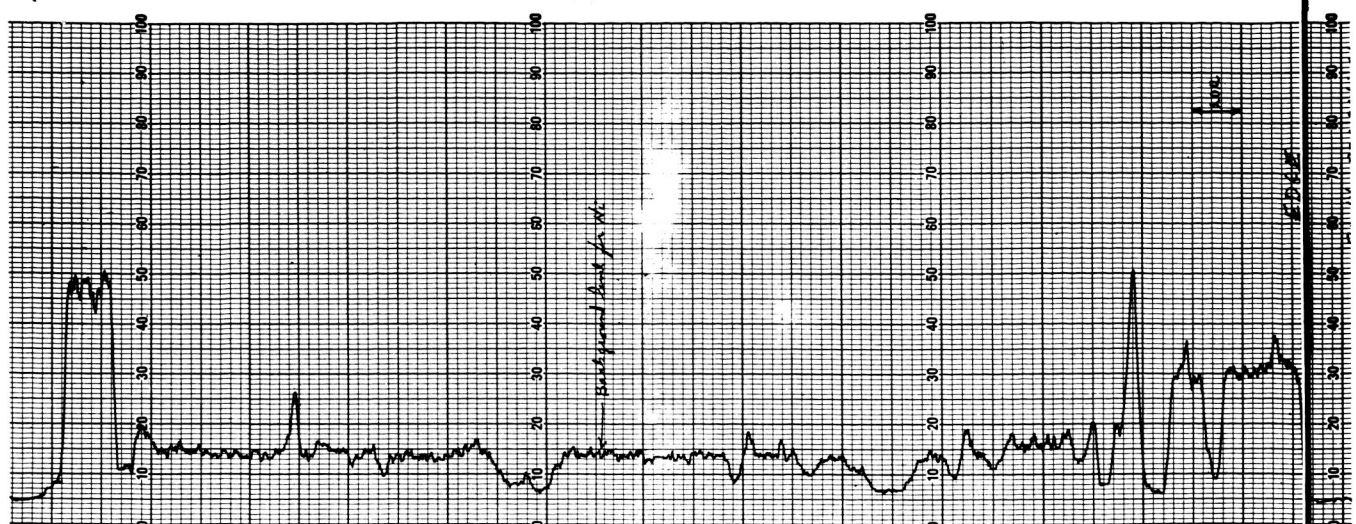


Nb Trace



Negative Replica of Photomicrograph Cross-section.

Figure 20. X-ray Microprobe Traces of Metal-Ceramic Seal.  
 Lucalox Metallized with Tungsten-yttria, and Brazed to Nb-1Zr  
 with Ni/Nb/Ti Alloy.  
 Traces Recorded with LiF Crystal, 25KV Accelerating Potential.



Ni Trace

Edge

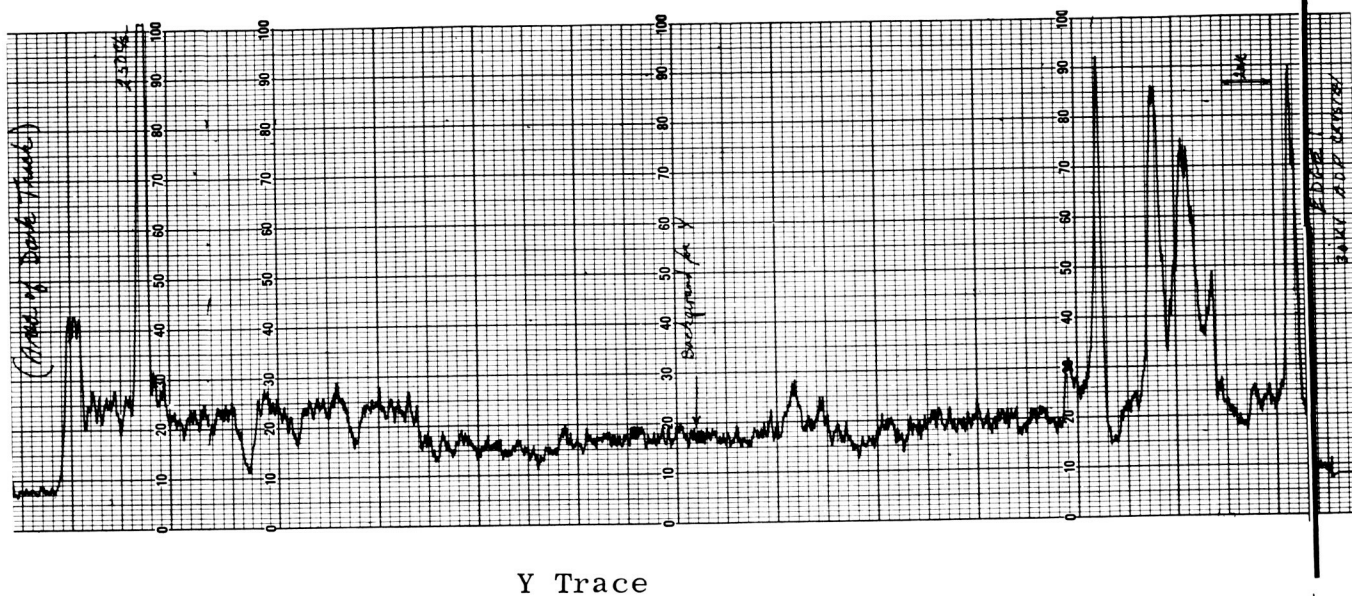
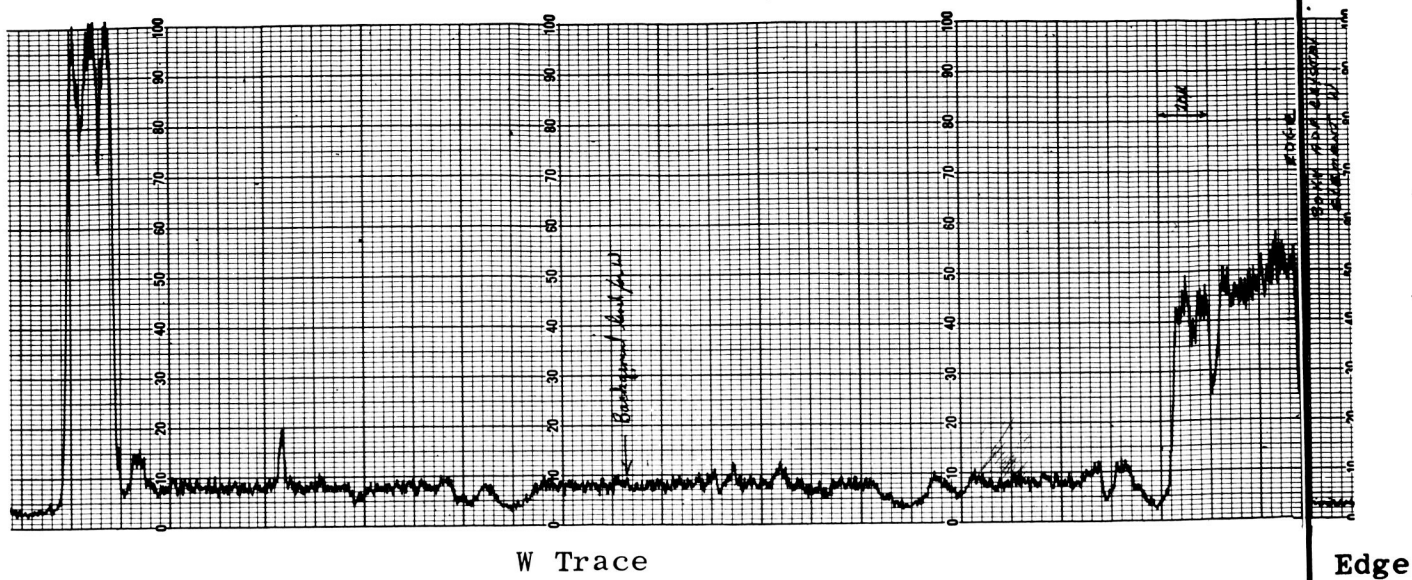


Al Trace



Negative Replica of Photomicrograph Cross-section.

Figure 21. X-ray Microprobe Traces of Metal-Ceramic Seal.  
 Lucalox Metallized with Tungsten-yttria, and Brazed to Nb-1Zr  
 with Ni/Nb/Ti Alloy.  
 Traces Recorded with ADP crystal, 30 KV accelerating potential.



Negative Replica of Photomicrograph Cross-section.

Figure 22. X-ray Microprobe Traces of Metal-Ceramic Seal.  
 Lucalox Metallized with Tungsten-yttria, and Brazed to Nb-1Zr  
 with Ni/Nb/Ti Alloy.  
 Traces Recorded with ADP Crystal, 30 KV Accelerating Potential.



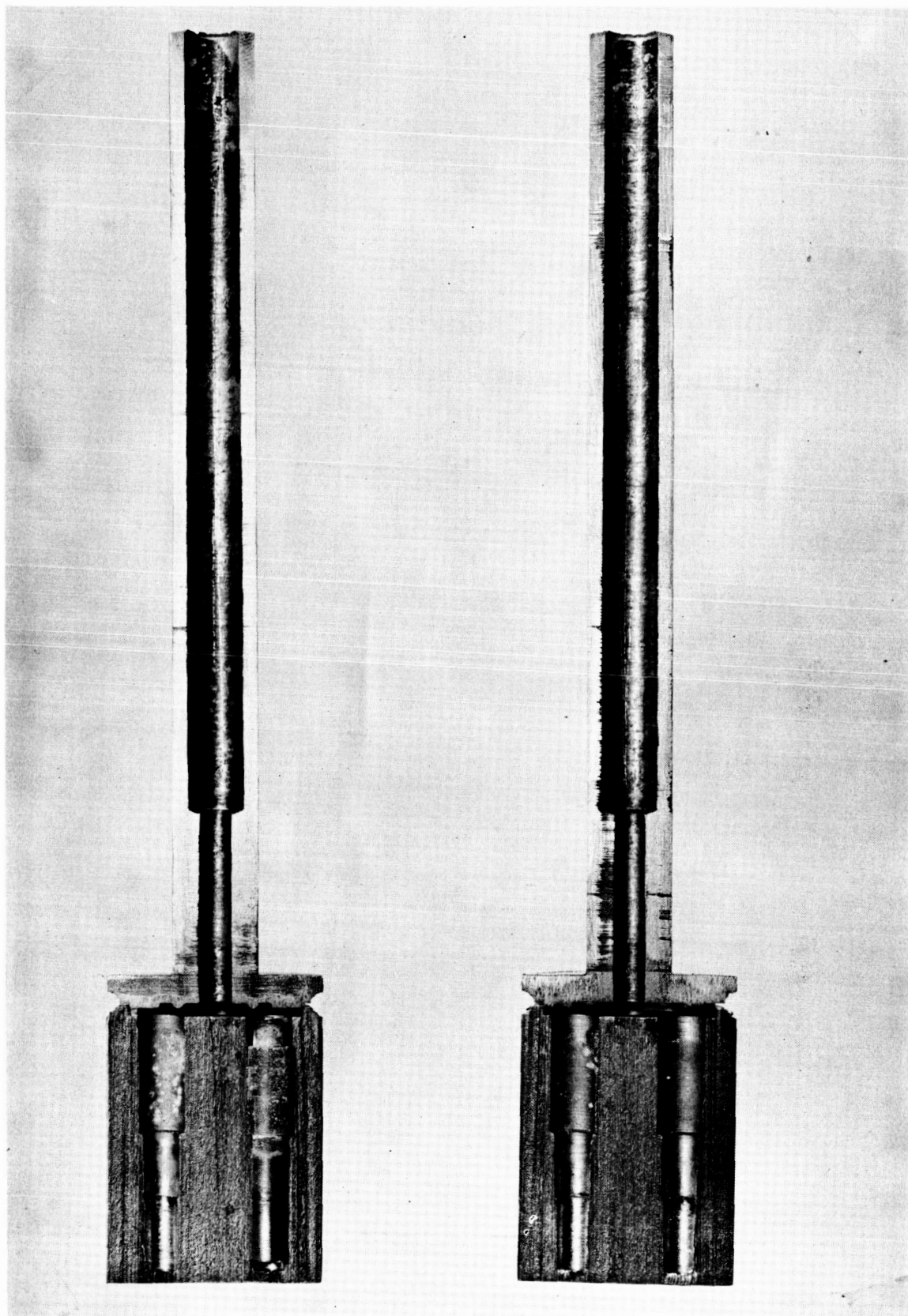


FIGURE 23

Terminal compatibility capsule in "as sectioned" condition after test with one terminal in place. (Full Scale)

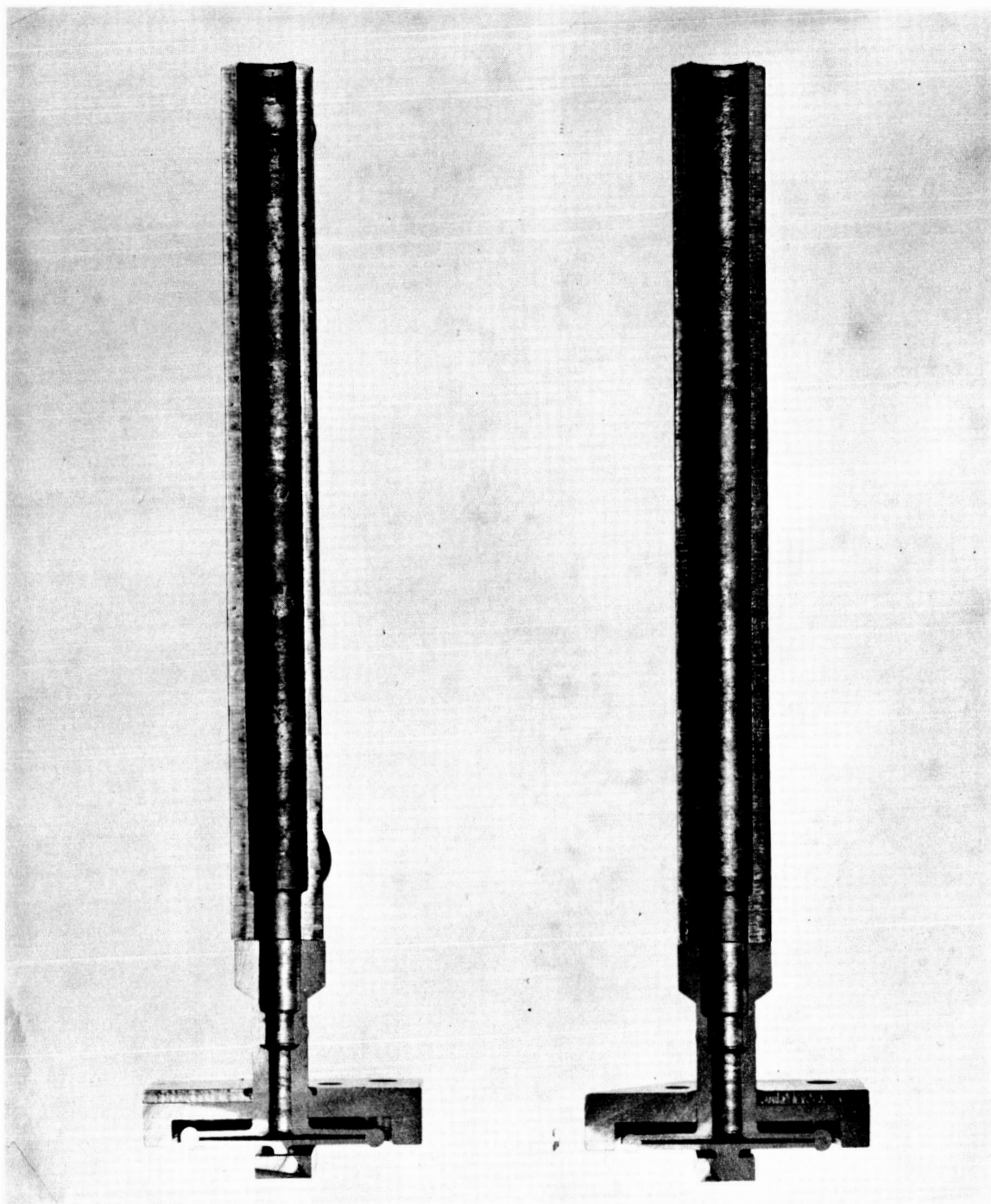


FIGURE 24

C-129Y compatibility capsule in "as sectioned" condition after test. (Full Scale)

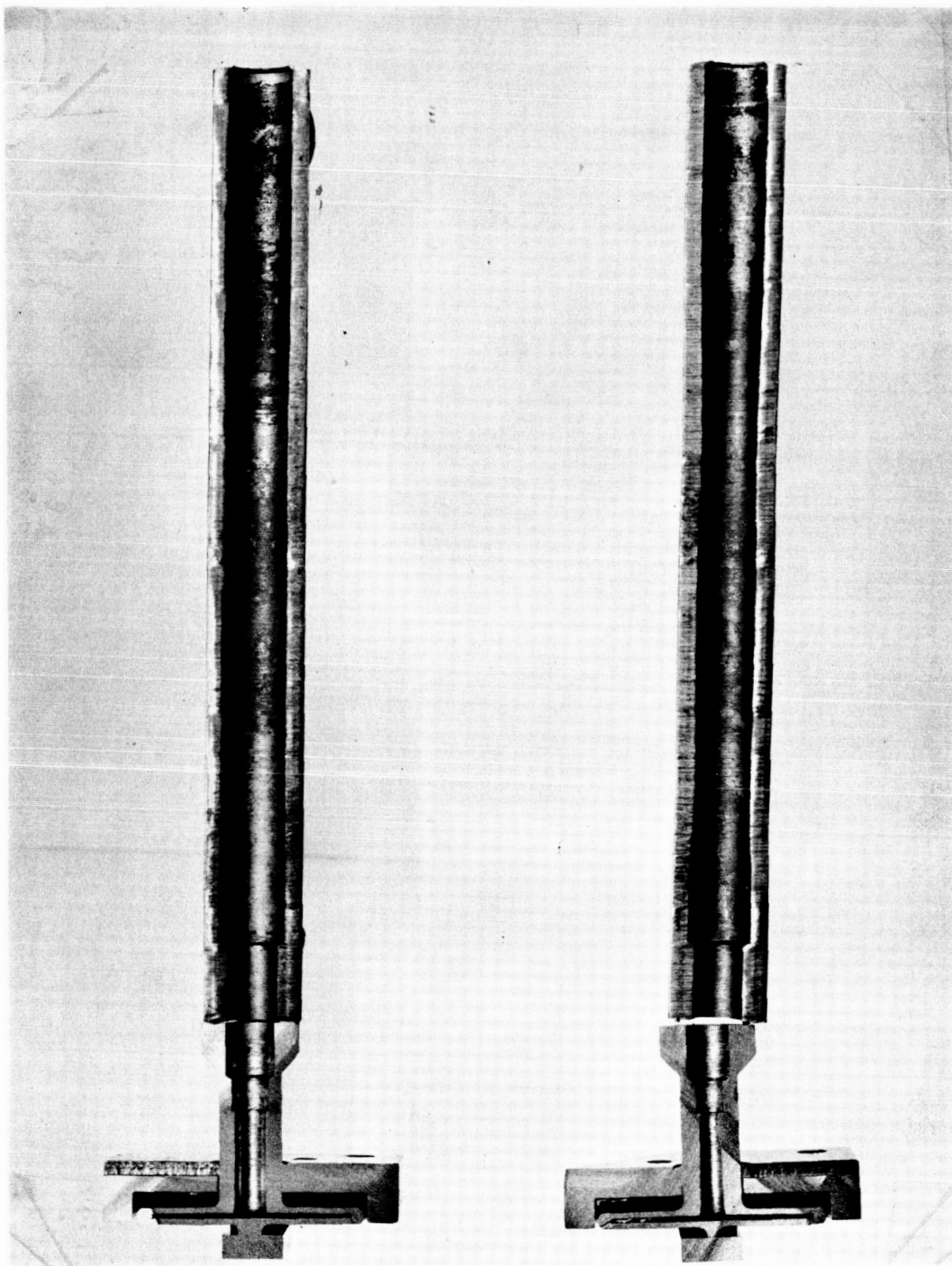


FIGURE 25

FS-85 compatibility capsule in "as sectioned" condition after test. (full scale)

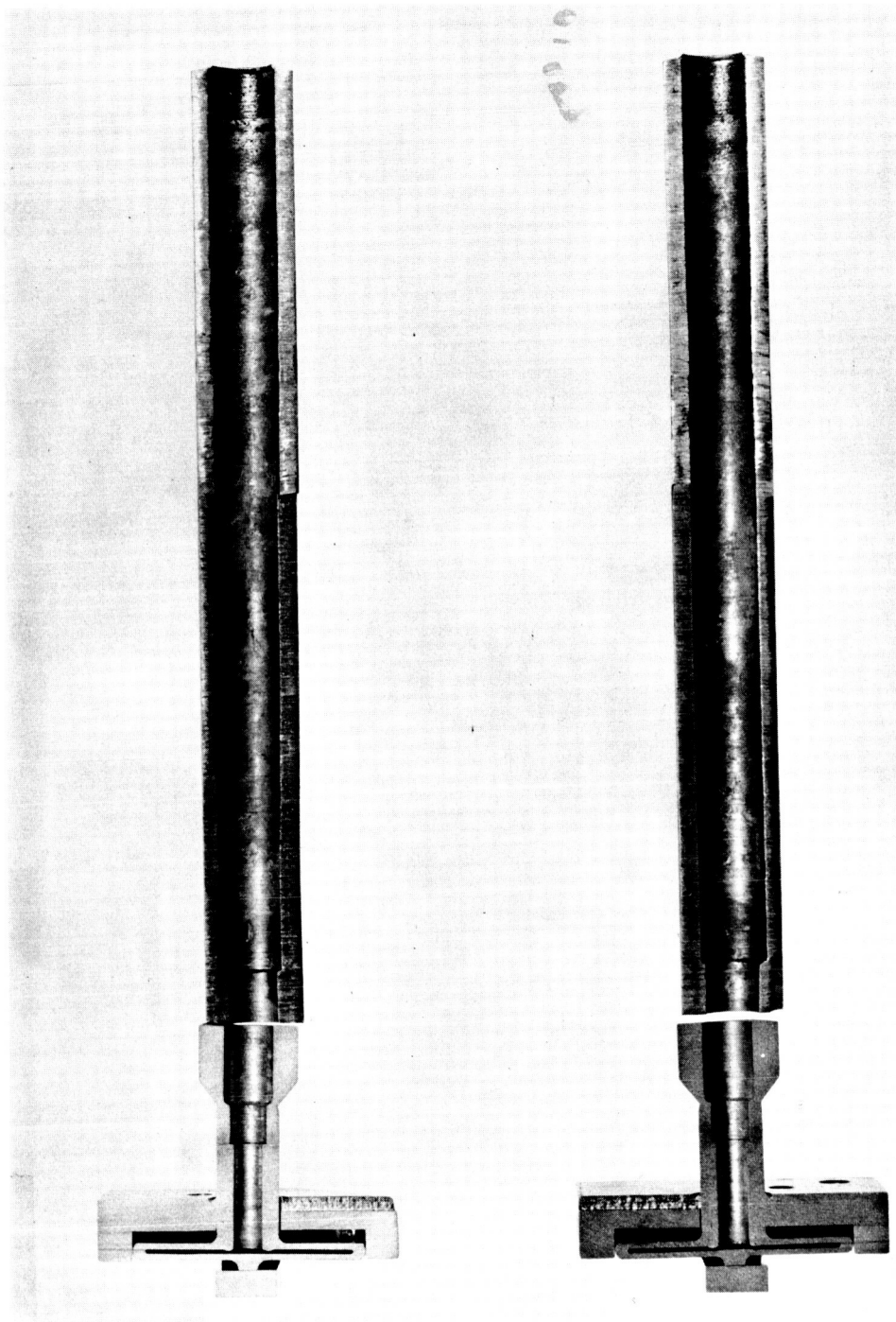


FIGURE 26

T-222 compatibility capsule in "as sectioned" condition after test. (Full Scale)



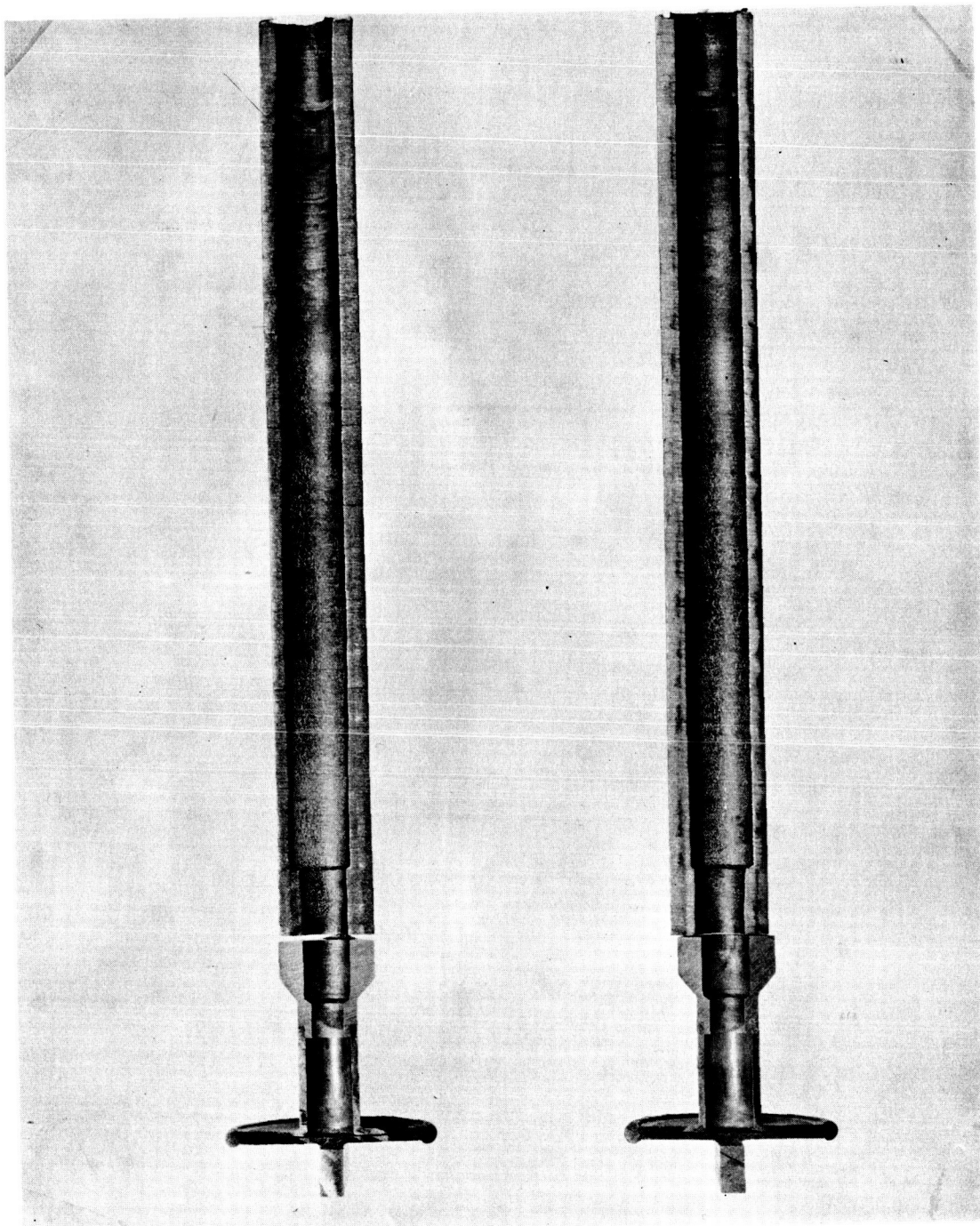


FIGURE 27

W-25 Re compatibility capsule in "as sectioned"  
condition after test. (Full Scale)

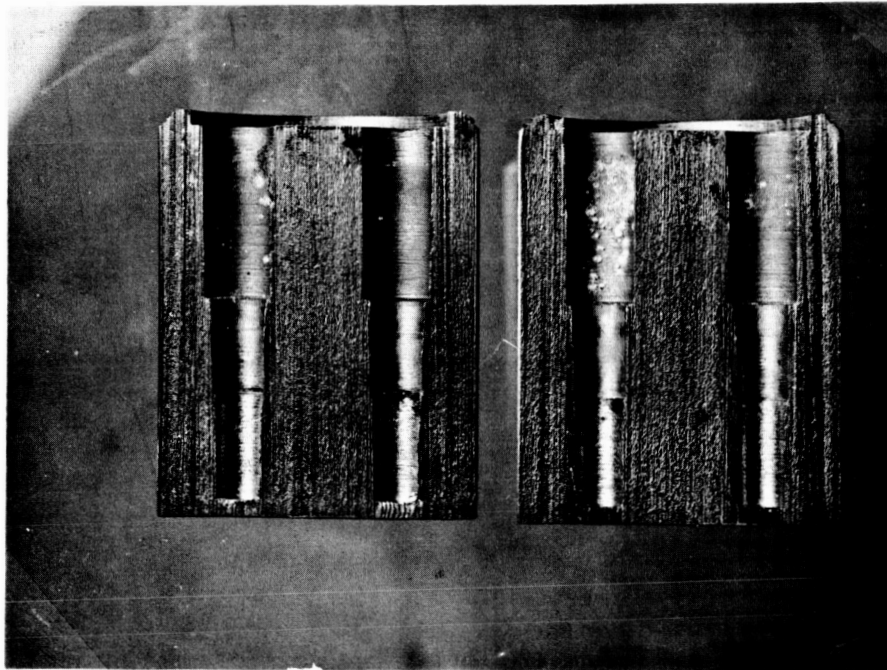
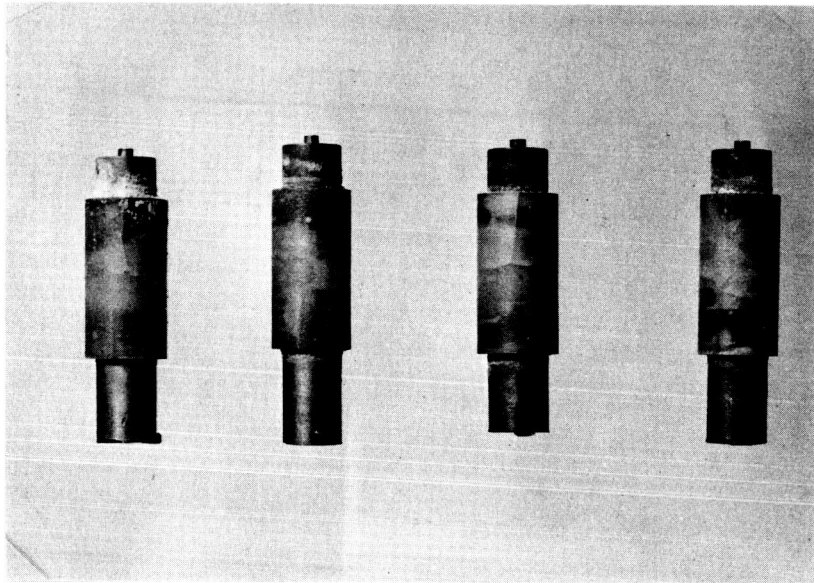


FIGURE 28

Lower portion of Terminal compatibility capsule in "as sectioned" condition after test with terminal removed.



**FIGURE 29**

**Electrical Terminals with lower end caps removed after test. (3X Magnification)**

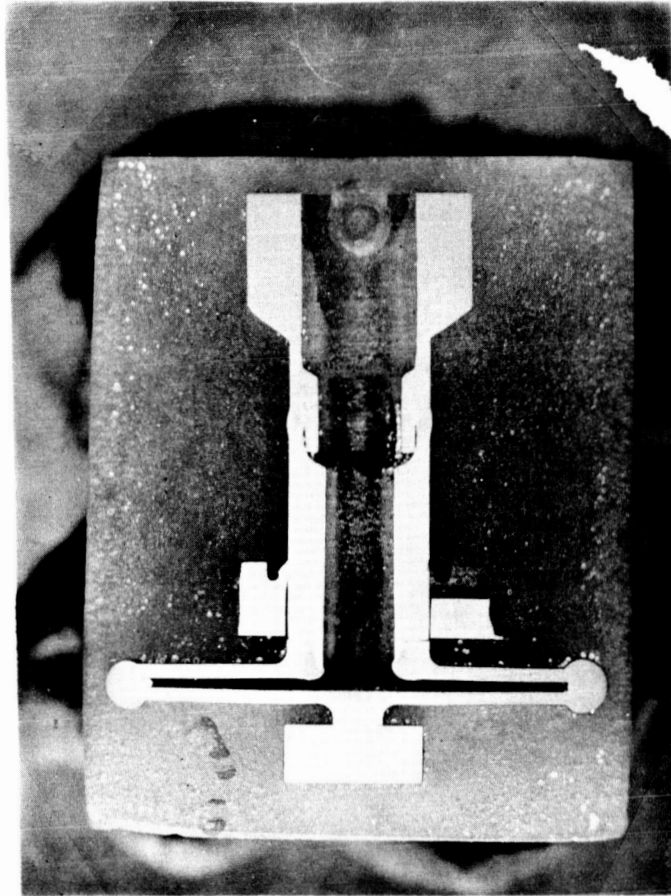


**FIGURE 30**

Photograph of C-129Y compatibility capsule after test with yoke removed. (3X Magnification)



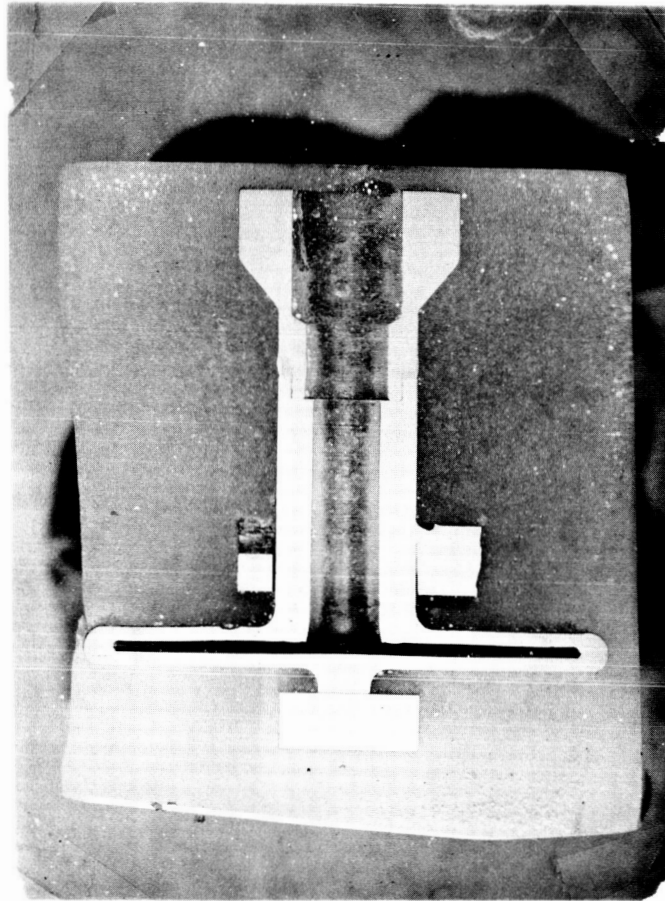


FIGURE 31

Photograph of FS-85 compatibility capsule after test with yoke removed. (3X Magnification)

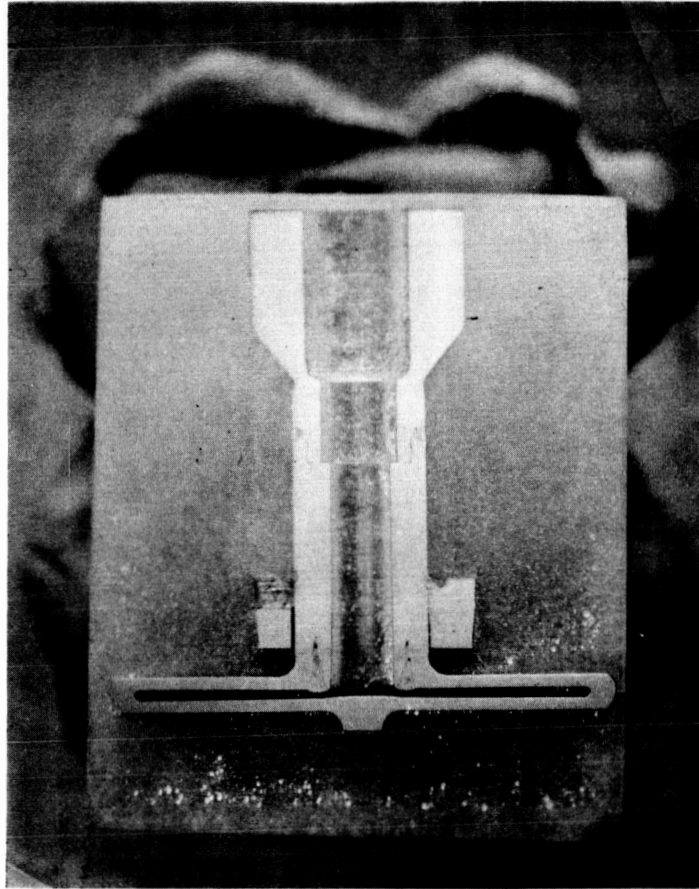
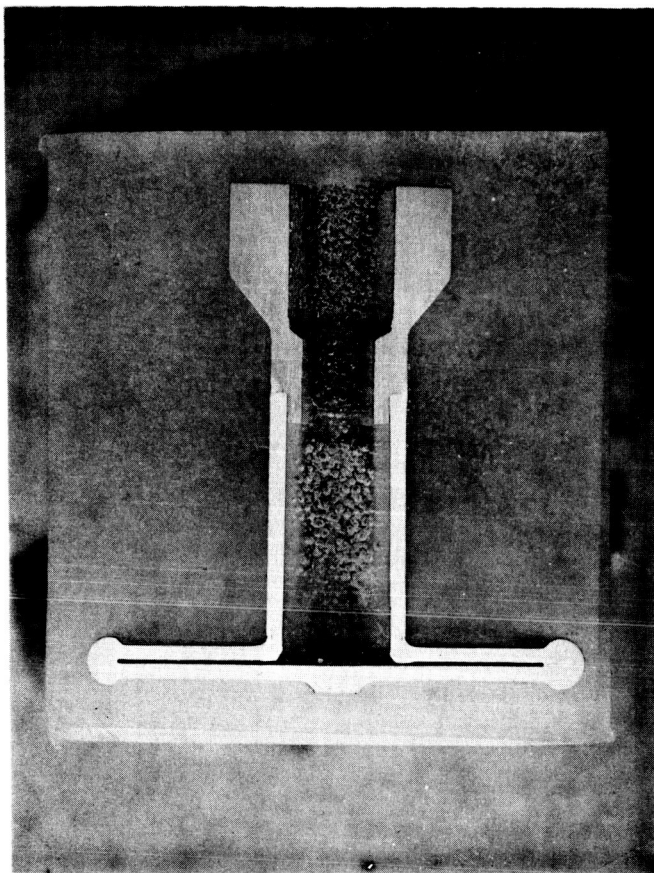


FIGURE 32

Photograph of T-222 compatibility capsule after test  
with yoke removed. (3X Magnification)



**FIGURE 33**

**Photograph of W-25 Re compatibility capsule after test  
with yoke removed. (3X Magnification)**

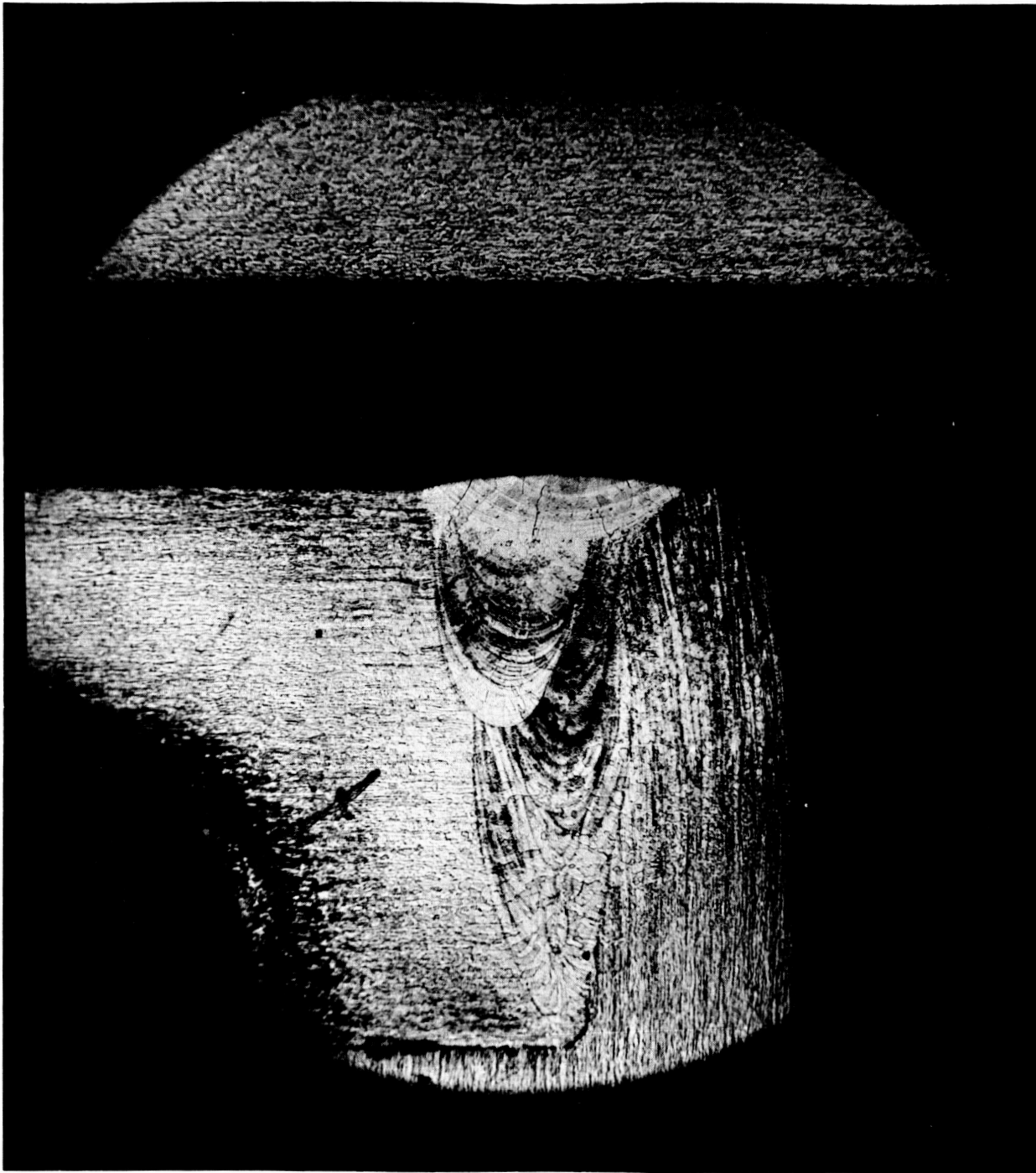


FIGURE 34

Photomicrograph of C-129Y compatibility capsule after test. Section shows electron-beam weld of C-129Y diaphragm to FS-85 tube, and portion of opposite diaphragm. (25X Magnification)

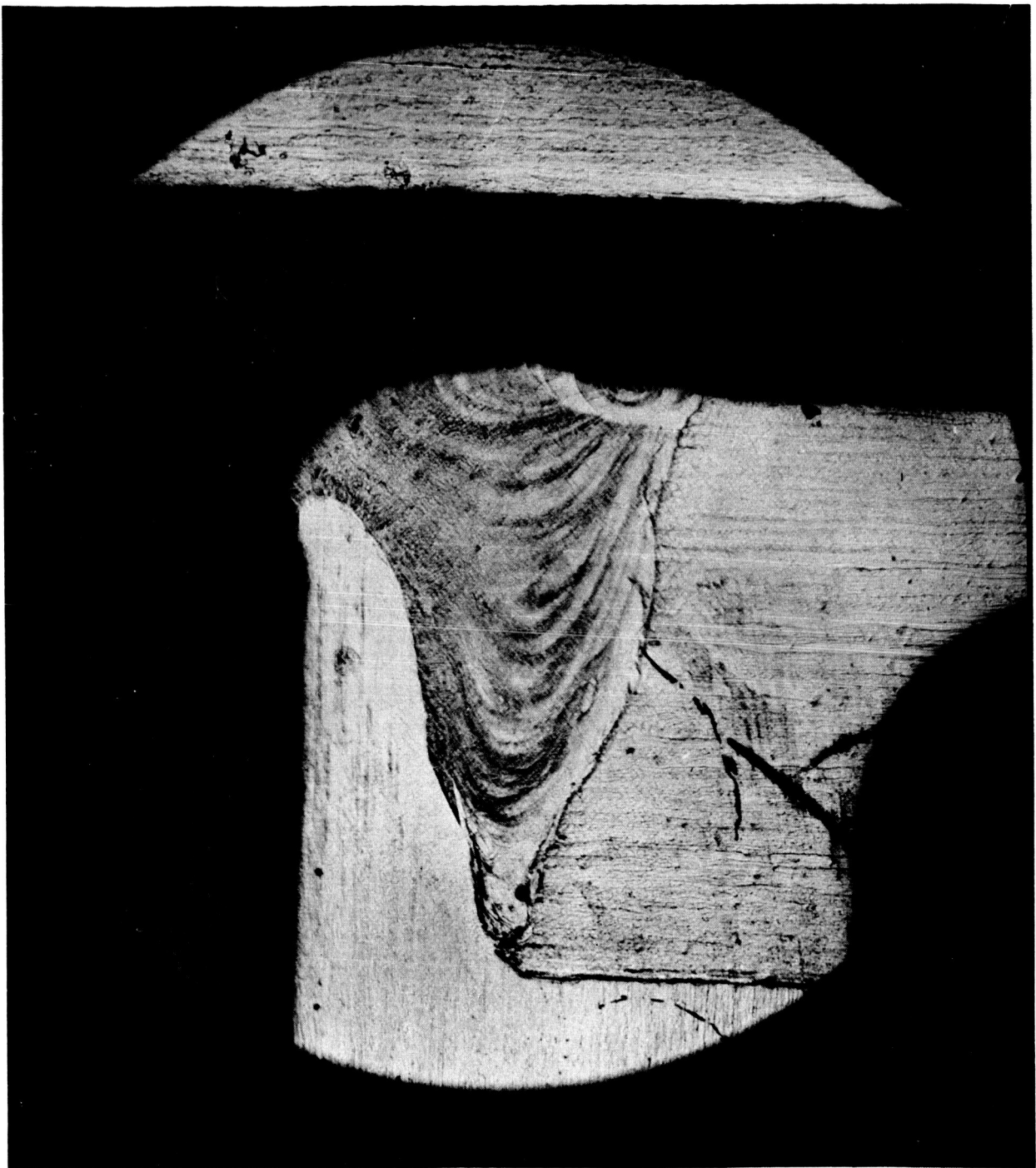


FIGURE 35

Photomicrograph of FS-85 compatibility capsule after test. (25X Magnification) Section shows electron-beam weld of FS-85 diaphragm to FS-85 tube, and portion of opposite diaphragm.

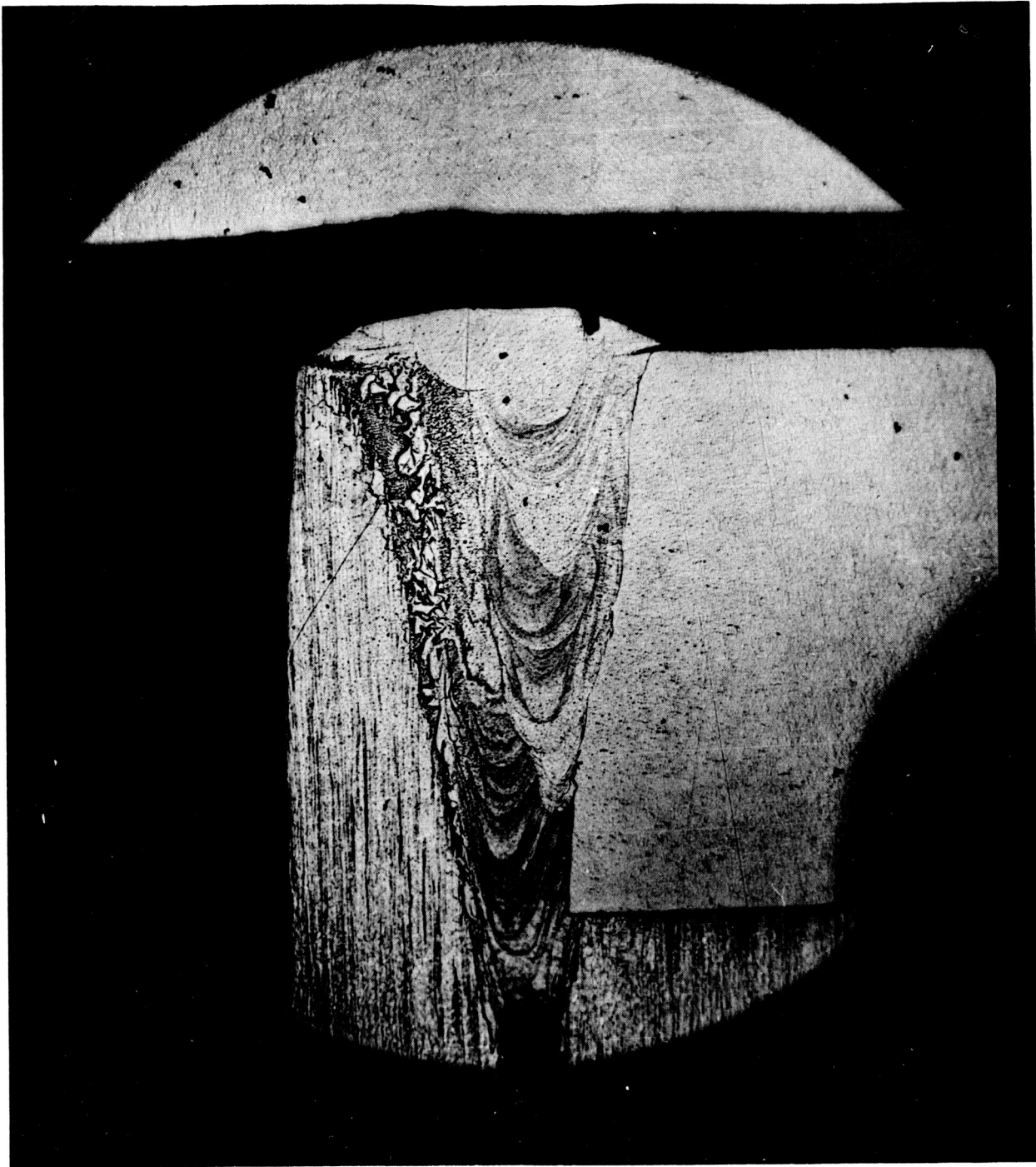


FIGURE 36

Photomicrograph of T-222 compatibility capsule after test. (25X magnification) Section shows electron-beam weld of T-222 diaphragm to FS-85 tube and portion of opposite diaphragm.

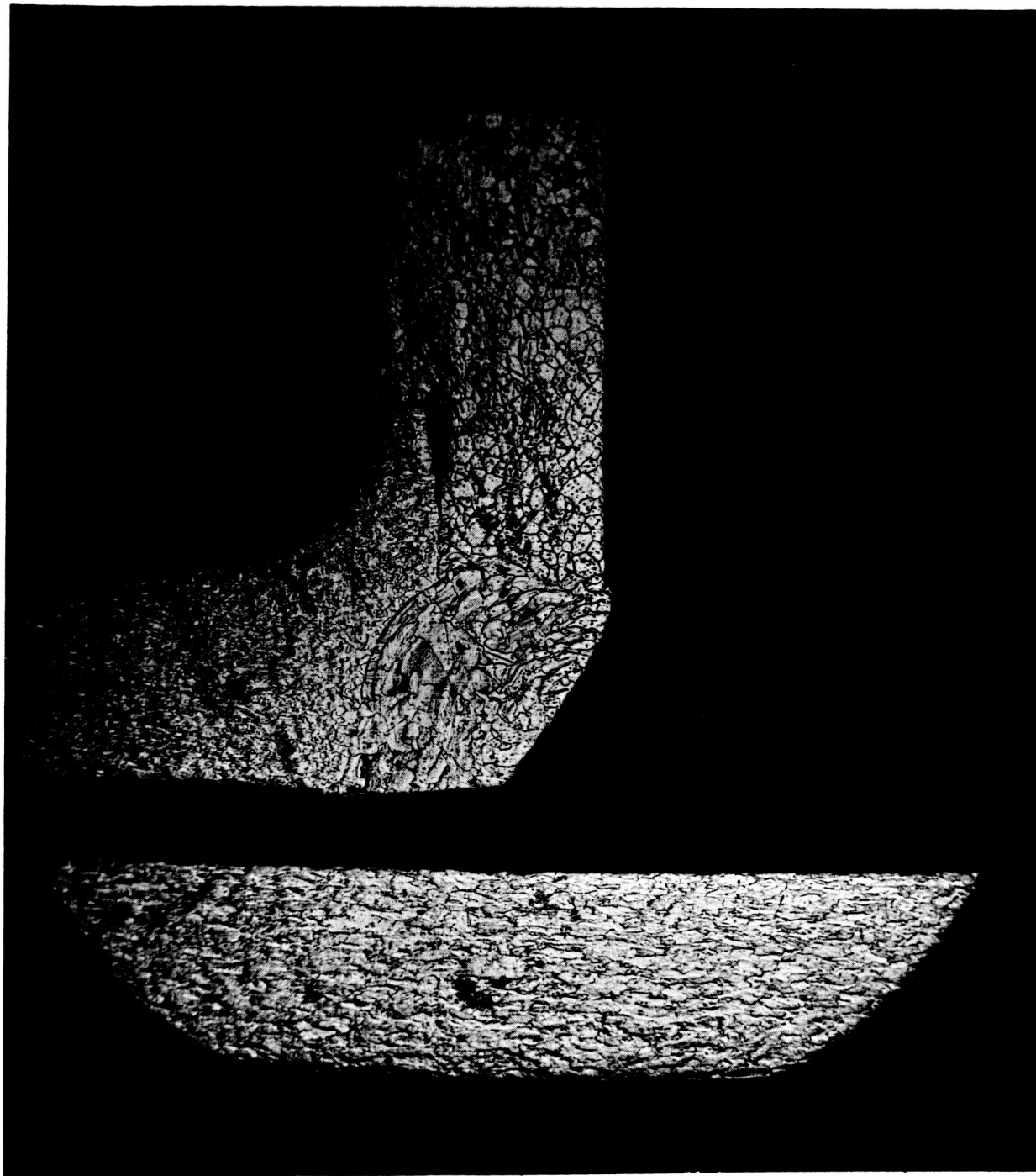


FIGURE 37

Photomicrograph of W-25 Re compatibility capsule after test.  
(25X magnification) Section shows electron-beam weld of W-25  
Re diaphragm to M0-50 Re tube and portion of opposite diaphragm.



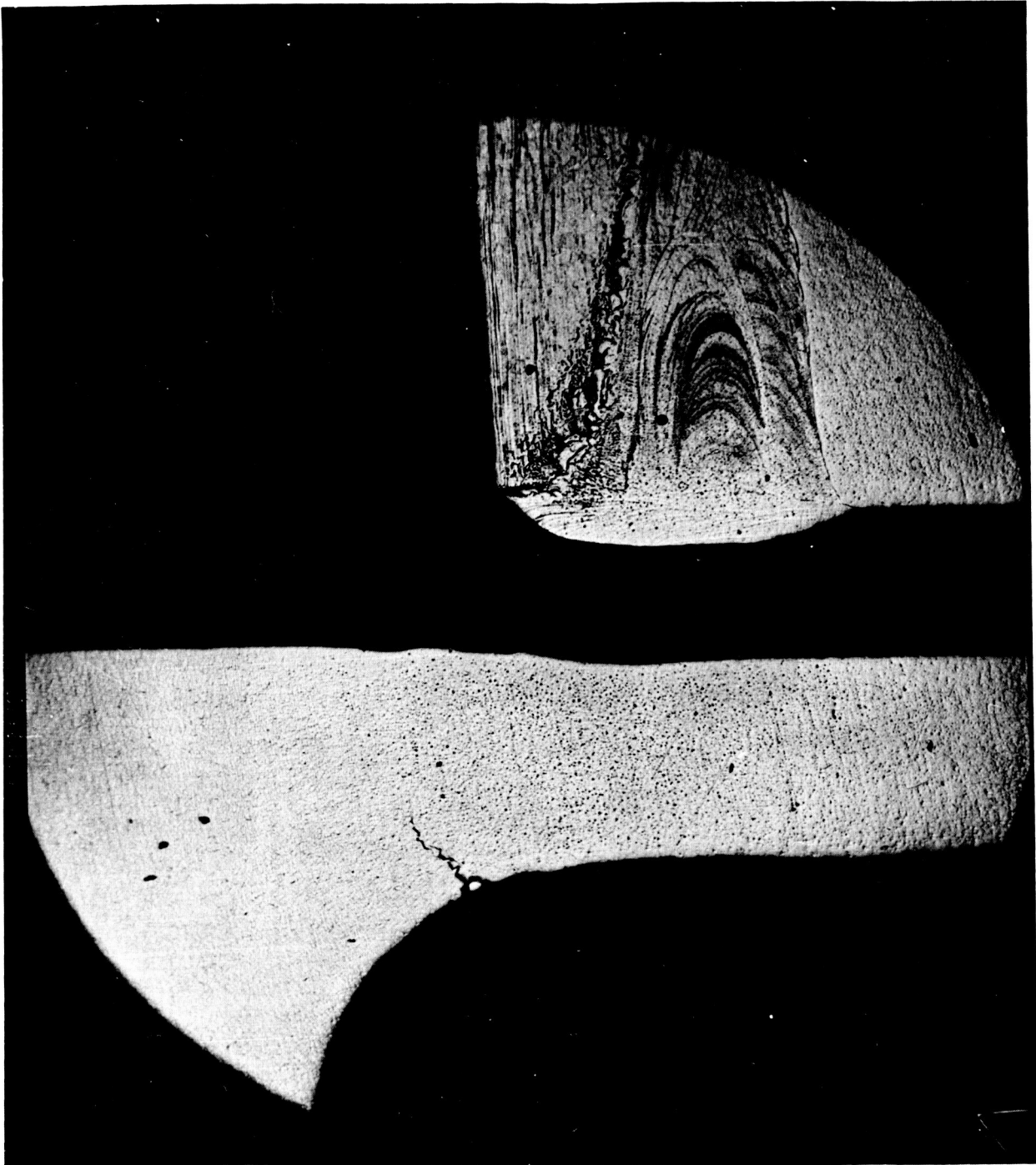


FIGURE 38

Intergranular crack in T-222 compatibility capsule at shoulder of boss in center of diaphragm. (25X magnification)



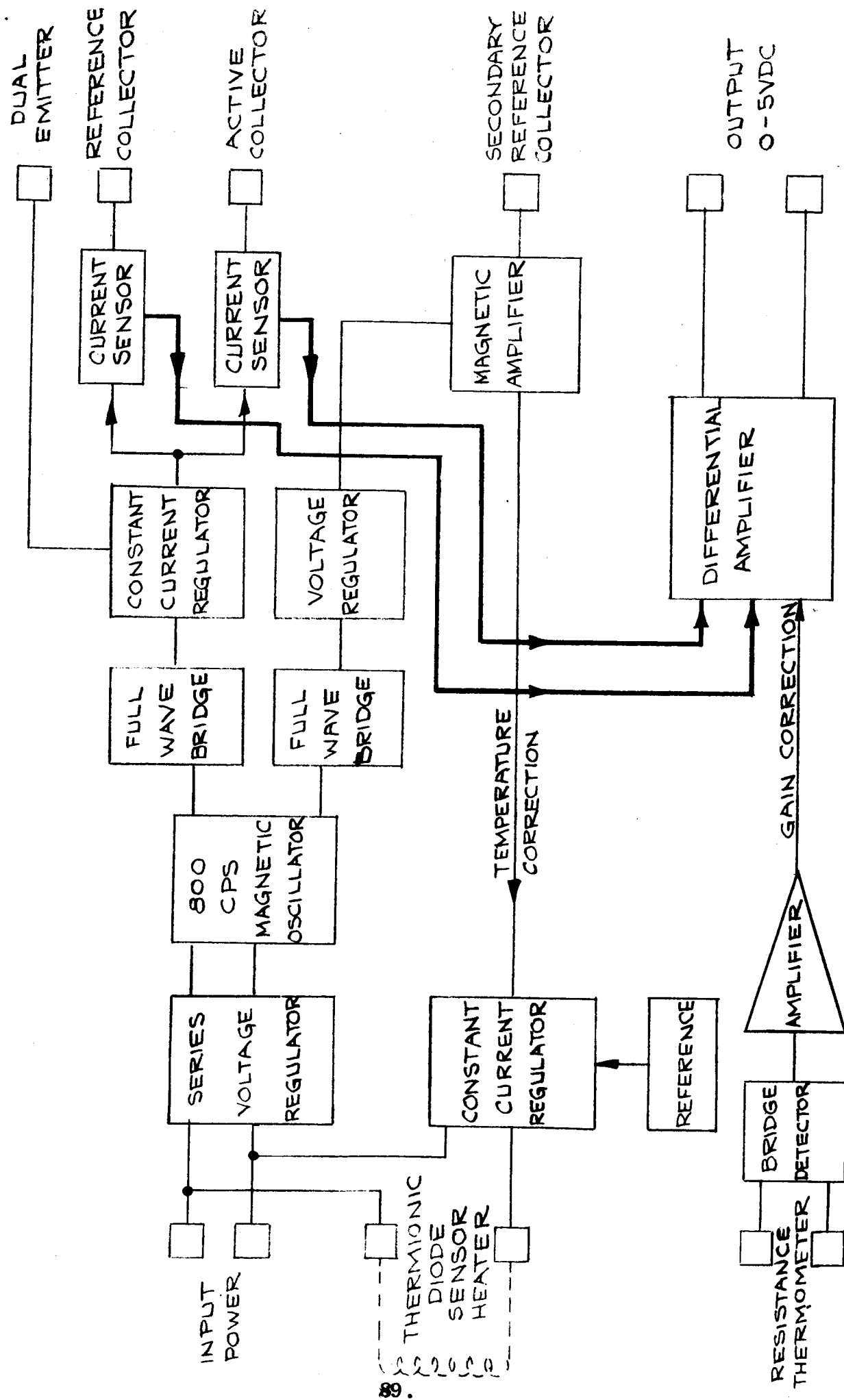
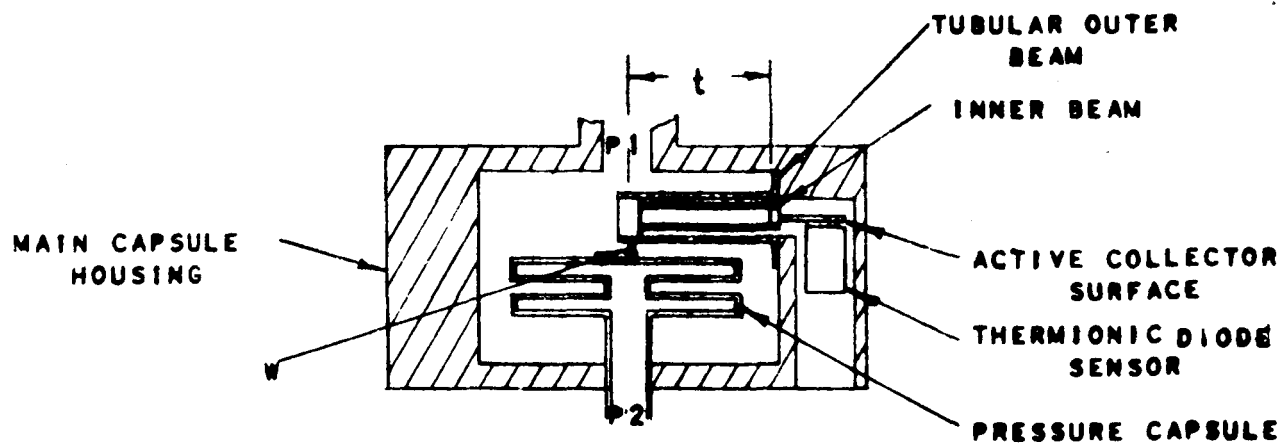
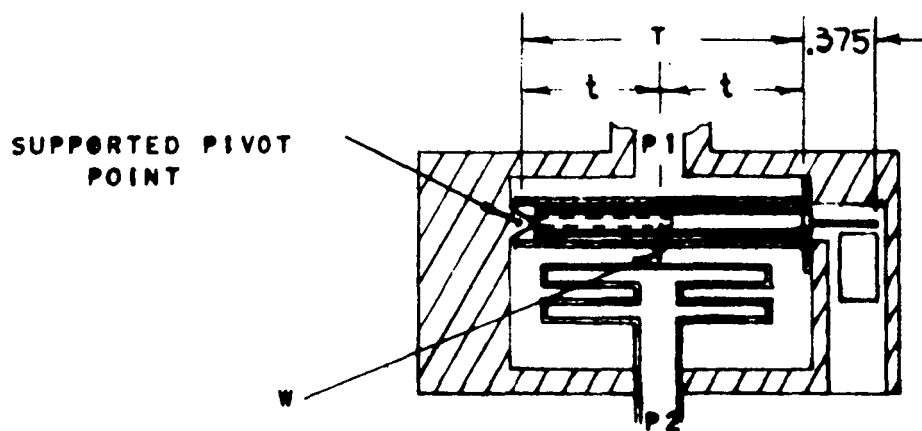


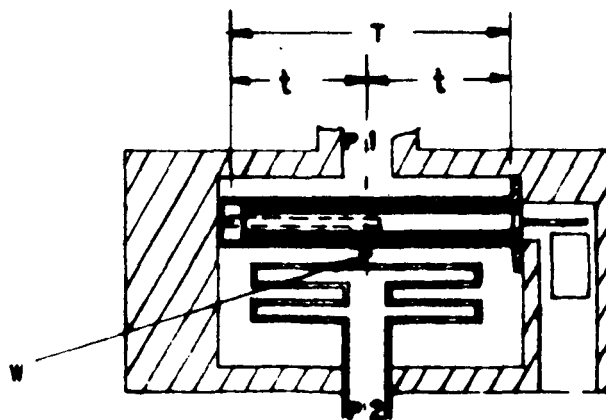
FIGURE 39  
TRANSDUCER SIGNAL CONDITIONING BLOCK DIAGRAM



CASE I - CANTILEVER, END LOAD



CASE II - END COUPLE, SUPPORTED PIVOT



CASE III - END COUPLE AND END LOAD

FIGURE 40

# DIFFERENTIAL PRESSURE TRANSDUCER CONFIGURATIONS

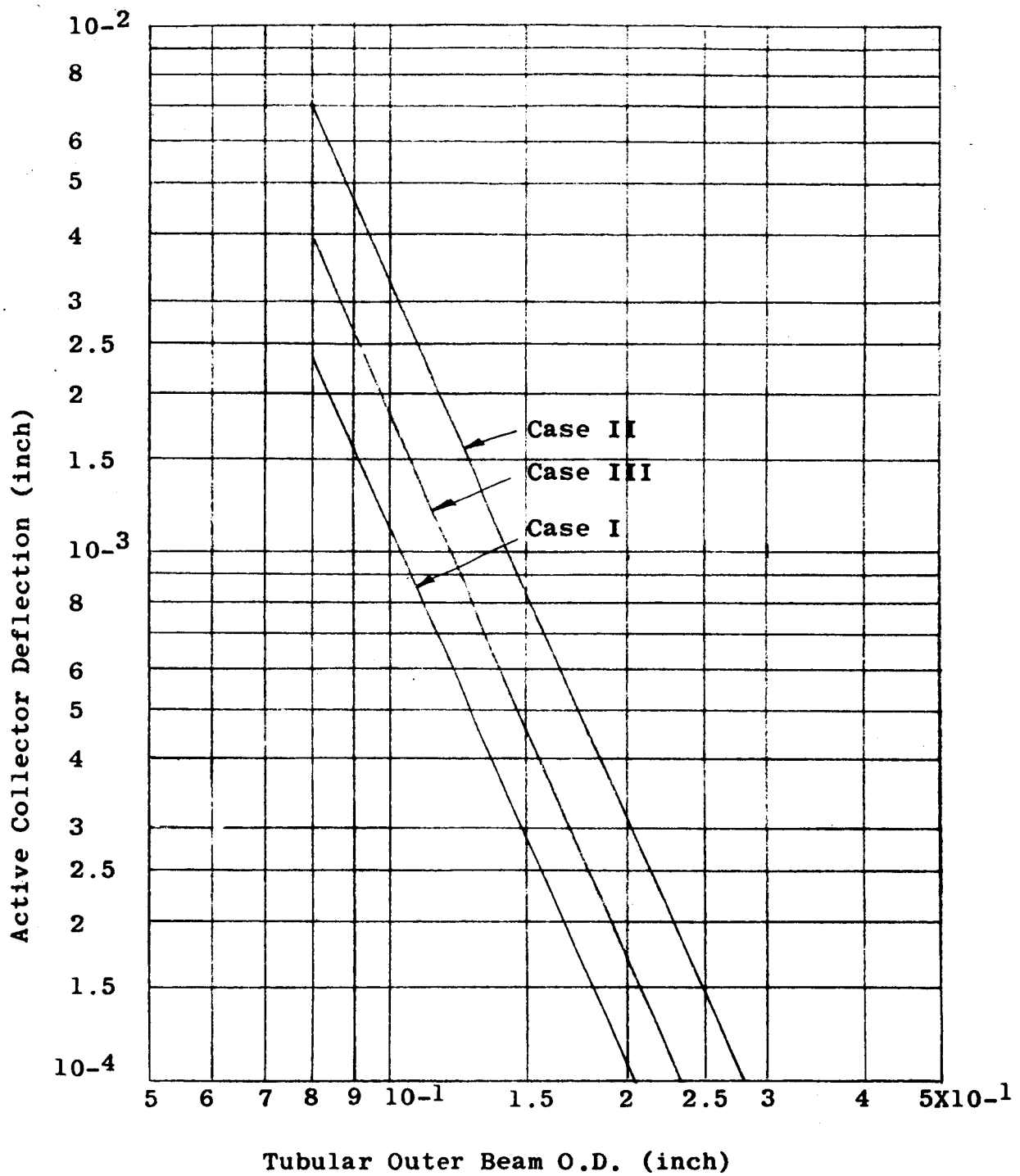


Figure 41  
Differential Pressure Transducer  
Deflection Characteristics

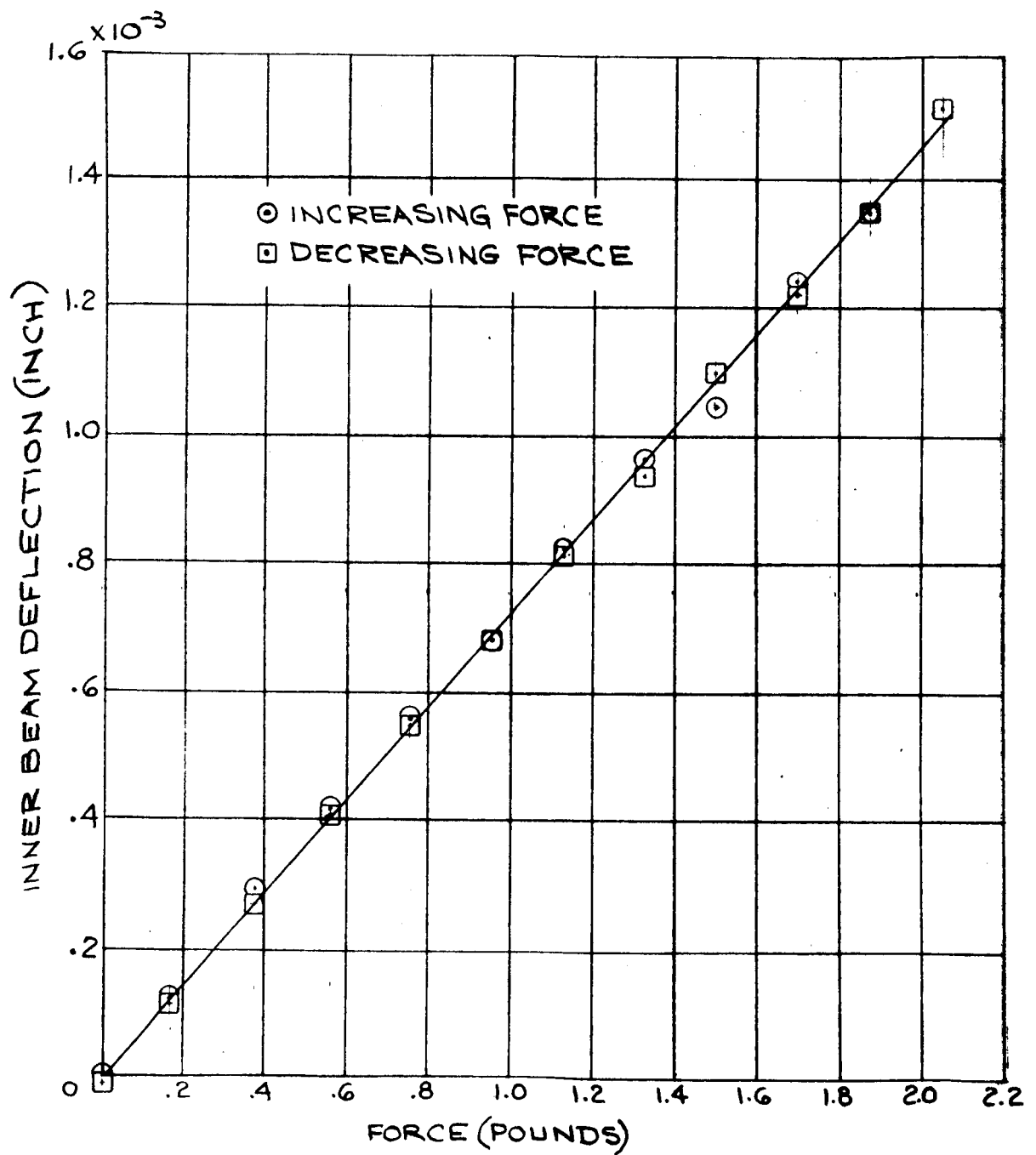


FIGURE 42  
DIFFERENTIAL MOCKUP  
FORCE-DEFLECTION CHARACTERISTIC

## LIST OF REFERENCES

1. Cassano, Anthony J.: Fifth Quarterly Report Pressure Measuring Systems for Closed Cycle Liquid Metal Facilities. NASA CR-54439, June 28, 1965.
2. Cassano, Anthony J.: Third Quarterly Report Pressure Measuring Systems for Closed Cycle Liquid Metal Facilities. NASA CR-54276, December 28, 1964.
3. Barton, J. R.: A Note on the Evaluation of Designs of Transducers for the Measurement of Dynamic Pressures in Liquid Systems. Statham Laboratories Instrument Notes No. 27, October 1958.
4. White, G. E.: Liquid Filled Pressure Gage Systems. Statham Laboratories Instrument Notes No. 7, October 1951.

APPENDIX A  
TRANSDUCER FREQUENCY RESPONSE

The initial portions of Appendix A are taken from References 3 and 4. This material has been extended by addition of the capillary tube model. By use of this model, the natural frequency and damping coefficient requirements may be satisfied simultaneously.

The natural frequency and the damping ratio are the two factors that define the dynamic movement of a mass subjected to a linear restoring force and viscous damping, and constrained to a single degree of freedom. Even though data is available concerning the natural frequency and damping ratio under a specified set of conditions (usually a natural frequency and damping ratio based upon the acceleration response of the pressure transducer in air), these data may be of little value in determining the frequency response under a different set of conditions. The natural frequency in air is determined by the actual moving mass and the spring constant of the

transducer. When there are no acoustical resonances, the natural frequency may be calculated by using the following equation:

$$f_n = \frac{1}{2\pi} \sqrt{\frac{K}{M}} \quad (A1)$$

where K is the spring constant and M is the moving mass of the transducer.

However, when this same transducer is connected (see Figure 1a) to a tube and the system (tube plus transducer) filled with a fluid of greater density than air, the natural frequency is significantly lower than the value determined experimentally in air, and is also lower than the calculated value given by Equation A1. In fact, the moving mass of the transducer may be an insignificant factor in determining the natural frequency of the system.

The calculation of the natural frequency and the damping ratio of a liquid-filled line plus transducer system is difficult. Even in a simplified analysis, it is necessary to know the parameters of the pressure

transducer and the liquid connections. The parameters of the liquid connections (i.e., density, temperature, viscosity, diameter and length of tube, elasticity of tube wall, etc.) are usually known or can be determined. However, the parameters of the transducer (i.e., spring constant, effective area of the sensing element, mass of moving components, volumetric displacement of sensing element, etc.) are difficult to obtain.

A method, based on a steady state measurement, will be presented whereby reasonable predictions may be calculated concerning the dynamic response of a liquid-filled system which is constrained to a single degree of freedom.

To do this, Equation A1 will be modified to take into consideration the effects of adding a connecting liquid-filled line to the basic transducer.

The pressure  $\Delta P$  required to displace the sensing element a distance  $\Delta x$  is given by

$$\Delta P = \frac{K \Delta x}{A} \quad (A2)$$



The volume change  $\Delta V$  accompanying this displacement is given by

$$\Delta V = A \Delta x \quad (A3)$$

Therefore,

$$\left( \frac{\Delta P}{\Delta V} \right) = \frac{K}{A^2} \quad (A4a)$$

and

$$K = \left( \frac{\Delta P}{\Delta V} \right) A^2 \quad (A4b)$$

For a laminar flow condition, the equivalent mass  $M_2$  of the liquid in the tube is given by

$$M_2 = \frac{4}{3} \rho a L \left( \frac{A}{a} \right)^2 = \frac{4}{3} \rho L \frac{A^2}{a} \quad (A5)$$

The total effective moving mass is

$$M = M_1 + M_2 \quad (A6)$$

Substitution of Equations A4b and A6 in Equation A1 yields

$$f_n = \frac{1}{2\pi} \sqrt{\frac{\left( \frac{\Delta P}{\Delta V} \right) A^2}{M_1 + M_2}} \quad (A7)$$

Replacing  $M_2$  in Equation A7 by its value from Equation A5, we have

$$f_n = \frac{1}{2\pi} \sqrt{\frac{\left(\frac{\Delta P}{\Delta V}\right) A^2}{M_1 + \frac{4}{3} \rho L \frac{A^2}{a}}} \quad (A8)$$

All the terms in Equation A8, except  $M_1$  and  $A$ , are known or can be determined by static measurement. If, as is usually true when using long, small-bore tubes, the mass  $M_1$  is small compared to  $M_2$ ,  $M_1$  can be neglected. Equation A8 now reduces to

$$f_n = \frac{1}{2\pi} \sqrt{\frac{\left(\frac{\Delta P}{\Delta V}\right) a}{\frac{4}{3} \rho L}} \quad (A9)$$

If it is desired to compute the transducer natural frequency then  $M_2$  can be considered negligible and

$$f_n = \frac{1}{2\pi} \sqrt{\frac{\left(\frac{\Delta P}{\Delta V}\right) A^2}{M_1}} \quad (A10)$$

The damping coefficient can be determined if the flow in the tube is assumed non-turbulent at the low

Reynolds numbers ordinarily encountered. For this condition, the velocity at the wall is zero and the velocity at the center of the tube is  $2u$ , with a parabolic distribution across the diameter.

$$u = \frac{A}{a} (\Delta \dot{x}) \quad (A11)$$

where  $(\Delta \dot{x})$  is the velocity of the sensing element.

The mass of the fluid in the tube is  $\rho aL$ . The kinetic energy of the fluid in the tube would be  $1/2(\rho aL u^2)$  if the flow were uniform. By integration across the area of the tube, the kinetic energy of the fluid can be found to be

$$\frac{1}{2} \cdot \frac{4}{3} \rho aL \left(\frac{A}{a}\right)^2 (\Delta \dot{x})^2 \quad (A12)$$

Therefore the equivalent mass of the fluid in the tube is

$$M_2 = \frac{4}{3} \rho aL \left(\frac{A}{a}\right)^2 \quad (A13)$$

If  $L \gg D$ , and the sensing element is in a large cavity, or is placed close to the tube entrance, the total effective mass is  $M = M_1 + M_2$  where  $M_2$  is usually the dominant term. End effects could be taken into account by using  $(L + D)$  as an approximate tube length. To compute the natural frequency of the system, the potential and kinetic energies are equated in the presence of a sinusoidal oscillation. Thus

$$\frac{1}{2} M \omega_n^2 = \frac{1}{2} K \quad (A14)$$

and

$$\omega_n = \sqrt{\frac{K}{M}} \quad (A15)$$

The effects of liquid viscosity may be approximated, since it is essential to know the amount of viscous damping in the system if the utmost in response fidelity is to be attained. By using the equation for viscous flow in a circular pipe, the pressure drop is

$$P = 32 \mu L \frac{u}{D^2} \quad (A16)$$

The average liquid velocity is

$$u = \frac{A (\dot{\Delta x})}{a} \quad (A17)$$

Then the pressure drop referred to the sensing element is

$$C (\dot{\Delta x}) = A_p = 32A\mu L \frac{A}{a} \frac{1}{D^2} (\dot{\Delta x}) \quad (A18)$$

Hence, the viscous reaction coefficient is

$$C = 8\pi L\mu \left(\frac{A}{a}\right)^2 \quad (A19)$$

The damping ratio for the system is then given by

$$h = 8\pi L\mu \frac{(A/a)^2}{2\sqrt{KM}} \quad (A20)$$

Substitution of the values for K and M from Equations A4b and A6 gives

$$h = \frac{4\pi L\mu \left(\frac{A}{a}\right)^2}{\sqrt{\left(\frac{\Delta P}{\Delta V}\right) A^2 \left[ M_1 + \frac{4}{3} \rho a L \left(\frac{A}{a}\right)^2 \right]}} \quad (A21)$$

Again, assuming  $M_1$  as small compared to  $M_2$ , and simplifying

$$h = \frac{2\pi \mu \sqrt{3} L}{(a)^{3/2} \sqrt{\left(\frac{\Delta P}{\Delta V}\right) \phi}} \quad (A22)$$

The solution of typical problems using the above equations will show that it is frequently difficult to obtain both the desired natural frequency and the damping coefficient at the same time. It is common practice to resolve this problem by the placement of some type of "snubber" element in the connecting line which will increase the influence of the tube viscous damping term without impairing the tube flow capability.

Figure 1b is a model similar to the original model of the pressure transducer piping system except that the connecting tubing consists of many parallel tubes.

For this physical model the changes that need to be considered are those that influence Equations A9 and

A22. For Equation A9 the terms to be considered are  $\left(\frac{\Delta P}{\Delta V}\right)$  and  $a$ . The total  $\left(\frac{\Delta P}{\Delta V}\right)$  is not changed for this new system and the area can be expressed as  $(N)\left(\frac{\pi d^2}{4}\right)$ . This simply means that for equivalent tube flow area the natural frequency is not changed. The equation for this situation is given by

$$f_n = \frac{1}{2\pi} \sqrt{\frac{\left(\frac{\Delta P}{\Delta V}\right) N \pi d^2}{\frac{4}{3} \rho L}} \quad (A23)$$

$$f_n = \left( \sqrt{\frac{3 \left(\frac{\Delta P}{\Delta V}\right)}{64 \pi}} \right) \left( \frac{1}{\sqrt{\rho}} \right) \left( d \sqrt{\frac{N}{L}} \right) \quad (A24)$$

Similarly the damping coefficient term (Equation A22) can be considered for the effects of the multiple tube arrangement on  $\left(\frac{\Delta P}{\Delta V}\right)$  and  $a$ . Since the tubes are in parallel, we can consider just one tube connected to a sensing element with  $N\left(\frac{\Delta P}{\Delta V}\right)$ . Since each portion of this new system will now be representative of the

total system, the damping term based on the elemental portion can be computed. For this case

$$h = \frac{2\pi \mu \sqrt{3L}}{\left(\frac{\pi d^2}{4}\right)^{3/2} \sqrt{\left(\frac{\Delta P}{\Delta V}\right) N \rho}} \quad (A25)$$

$$h = \left(16 \sqrt{\frac{3}{\pi \left(\frac{\Delta P}{\Delta V}\right)}}\right) \left(\frac{\mu}{\sqrt{\rho}}\right) \left(\frac{1}{d^3} \sqrt{\frac{L}{N}}\right) \quad (A26)$$

The use of these equations coupled with standard amplitude ratio and phase angle curves will provide the basis for predicting transducer response characteristics. It is recommended the Equation A10 be used as a check on the assumption that  $M_1$  can be neglected. If this term is not negligible it can be factored into the analysis when developing the attenuation-phase diagram.

The main limitation on the above analysis is that fluid compressibility and the resultant distributive capacitance is not considered.



## APPENDIX B

### NOMENCLATURE

- A = effective area of the sensing element
- a = cross sectional area of the connecting tube
- D = diameter of the connecting tube of Figure 1a
- d = diameter of individual tube of Figure 1b
- $f_n$  = natural frequency, cycles per second
- h = damping ratio
- K = spring constant
- L = length of the connecting tube
- $M_1$  = moving mass of the transducer
- $M_2$  = equivalent mass of the liquid
- N = number of tubes, see Figure 1b
- $\Delta P$  = pressure change
- $P_1, P_2$  = pressures whose differential is to be monitored, see Figure 40
- T = tubular outer beam length, Cases II & III of Figure 40
- t = tubular outer beam length, Case I of Figure 40
- u = average velocity of fluid in the tube
- $\Delta V$  = volume change
- W = force exerted by pressure capsule on beam, see Figure 40

$\Delta x$  = displacement of the sensing element

$\mu$  = liquid viscosity

$\rho$  = liquid density

$\omega_n$  = natural frequency, rad./sec.